

GRAVITATIONAL WAVES FROM KNOWN PULSARS: RESULTS FROM THE INITIAL DETECTOR ERA

J. AASI¹, J. ABADIE¹, B. P. ABBOTT¹, R. ABBOTT¹, T. ABBOTT², M. R. ABERNATHY¹, T. ACCADIA³, F. ACERNESE^{4,5}, C. ADAMS⁶, T. ADAMS⁷, R. X. ADHIKARI¹, C. AFFELDT⁸, M. AGATHOS⁹, N. AGGARWAL¹⁰, O. D. AGUIAR¹¹, P. AJITH¹, B. ALLEN^{8,12,13}, A. ALLOCCA^{14,15}, E. AMADOR CERON¹², D. AMARIUTEI¹⁶, R. A. ANDERSON¹, S. B. ANDERSON¹, W. G. ANDERSON¹², K. ARAI¹, M. C. ARAYA¹, C. ARCENEUX¹⁷, J. AREEDA¹⁸, S. AST¹³, S. M. ASTON⁶, P. ASTONE¹⁹, P. AUFMUTH¹³, C. AULBERT⁸, L. AUSTIN¹, B. E. AYLOTT²⁰, S. BABAK²¹, P. T. BAKER²², G. BALLARDIN²³, S. W. BALLMER²⁴, J. C. BARAYOGA¹, D. BARKER²⁵, S. H. BARNUM¹⁰, F. BARONE^{4,5}, B. BARR²⁶, L. BARSOTTI¹⁰, M. BARSUGLIA²⁷, M. A. BARTON²⁵, I. BARTOS²⁸, R. BASSIRI^{26,29}, A. BASTI^{14,30}, J. BATCH²⁵, J. BAUCHROWITZ⁸, TH. S. BAUER⁹, M. BEBRONNE³, B. BEHNKE²¹, M. BEJGER³¹, M. G. BEKER⁹, A. S. BELL²⁶, C. BELL²⁶, I. BELOPOLSKI²⁸, G. BERGMANN⁸, J. M. BERLINER²⁵, D. BERSANETTI^{32,33}, A. BERTOLINI⁹, D. BESSIS³⁴, J. BETZWIESER⁶, P. T. BEYERSDORF³⁵, T. BHADBHADRE²⁹, I. A. BILENKO³⁶, G. BILLINGSLEY¹, J. BIRCH⁶, M. BITOSI¹⁴, M. A. BIZOUARD³⁷, E. BLACK¹, J. K. BLACKBURN¹, L. BLACKBURN³⁸, D. BLAIR³⁹, M. BLOM⁹, O. BOCK⁸, T. P. BODIYA¹⁰, M. BOER⁴⁰, C. BOGAN⁸, C. BOND²⁰, F. BONDU⁴¹, L. BONELLI^{14,30}, R. BONNAND⁴², R. BORK¹, M. BORN⁸, V. BOSCHI¹⁴, S. BOSE⁴³, L. BOSI⁴⁴, J. BOWERS², C. BRADASCHIA¹⁴, P. R. BRADY¹², V. B. BRAGINSKY³⁶, M. BRANCHESI^{45,46}, C. A. BRANNEN⁴³, J. E. BRAU⁴⁷, J. BREYER⁸, T. BRIANT⁴⁸, D. O. BRIDGES⁶, A. BRILLET⁴⁰, M. BRINKMANN⁸, V. BRISSON³⁷, M. BRITZGER⁸, A. F. BROOKS¹, D. A. BROWN²⁴, D. D. BROWN²⁰, F. BRÜCKNER²⁰, T. BULIK⁴⁹, H. J. BULTEN^{9,50}, A. BUONANNO⁵¹, D. BUSKULIC³, C. BUY²⁷, R. L. BYER²⁹, L. CADONATI⁵², G. CAGNOLI⁴², J. CALDERÓN BUSTILLO⁵³, E. CALLONI^{4,54}, J. B. CAMP³⁸, P. CAMPSIE²⁶, K. C. CANNON⁵⁵, B. CANUEL²³, J. CAO⁵⁶, C. D. CAPANO⁵¹, F. CARBOGNANI²³, L. CARBONE²⁰, S. CARIDE⁵⁷, A. CASTIGLIA⁵⁸, S. CAUDILL¹², M. CAVAGLIÀ¹⁷, F. CAVALIER³⁷, R. CAVALIERI²³, G. CELLA¹⁴, C. CEPEDA¹, E. CESARINI⁵⁹, R. CHAKRABORTY¹, T. CHALERMSONGSAK¹, S. CHAO⁶⁰, P. CHARLTON⁶¹, E. CHASSANDE-MOTTIN²⁷, X. CHEN³⁹, Y. CHEN⁶², A. CHINCARINI³², A. CHIUMMO²³, H. S. CHO⁶³, J. CHOW⁶⁴, N. CHRISTENSEN⁶⁵, Q. CHU³⁹, S. S. Y. CHUA⁶⁴, S. CHUNG³⁹, G. CIANI¹⁶, F. CLARA²⁵, D. E. CLARK²⁹, J. A. CLARK⁵², F. CLEVA⁴⁰, E. COCCIA^{66,67}, P.-F. COHADON⁴⁸, A. COLLA^{19,68}, M. COLOMBINI⁴⁴, M. CONSTANCIO JR.¹¹, A. CONTE^{19,68}, R. CONTE⁶⁹, D. COOK²⁵, T. R. CORBITT², M. CORDIER³⁵, N. CORNISH²², A. CORSI⁷⁰, C. A. COSTA¹¹, M. W. COUGHLIN⁷¹, J.-P. COULON⁴⁰, S. COUNTRYMAN²⁸, P. COUVARES²⁴, D. M. COWARD³⁹, M. COWART⁷, D. C. COYNE¹, K. CRAIG²⁶, J. D. E. CREIGHTON¹², T. D. CREIGHTON³⁴, S. G. CROWDER⁷², A. CUMMING²⁶, L. CUNNINGHAM²⁶, E. CUOCO²³, K. DAHL⁸, T. DAL CANTON⁸, M. DAMJANIC⁸, S. L. DANILISHIN³⁹, S. D'ANTONIO⁵⁹, K. DANZMANN^{8,13}, V. DATTILO²³, B. DAUDERT¹, H. DAVELOZA³⁴, M. DAVIER³⁷, G. S. DAVIES²⁶, E. J. DAW⁷³, R. DAY²³, T. DAYANGA⁴³, R. DE ROSA^{4,54}, G. DEBRECZENI⁷⁴, J. DEGALLAIX⁴², W. DEL POZZO⁹, E. DELEEUW¹⁶, S. DELÉGLISE⁴⁸, T. DENKER⁸, T. DENT⁸, H. DERELI⁴⁰, V. DERGACHEV¹, R. DEROSA², R. DESALVO⁶⁹, S. DHURANDHAR⁷⁵, L. DI FIORE⁴, A. DI LIETO^{14,30}, I. DI PALMA⁸, A. DI VIRGILIO¹⁴, M. DÍAZ³⁴, A. DIETZ¹⁷, K. DMITRY³⁶, F. DONOVAN¹⁰, K. L. DOOLEY⁸, S. DORAVARI⁶, M. DRAGO^{76,77}, R. W. P. DREVER⁷⁸, J. C. DRIGGERS¹, Z. DU⁵⁶, J.-C. DUMAS³⁹, S. DWYER²⁵, T. EBERLE⁸, M. EDWARDS⁷, A. EFFLER², P. EHRENS¹, J. EICHHOLZ¹⁶, S. S. EIKENBERRY¹⁶, G. ENDRŐCZI⁷⁴, R. ESSICK¹⁰, T. ETZEL¹, K. EVANS²⁶, M. EVANS¹⁰, T. EVANS⁶, M. FACTOUROVICH²⁸, V. FAFONE^{59,67}, S. FAIRHURST⁷, Q. FANG³⁹, S. FARINON³², B. FARR⁷⁹, W. FARR⁷⁹, M. FAVATA⁸⁰, D. FAZI⁷⁹, H. FEHRMANN⁸, D. FELDBAUM^{6,16}, I. FERRANTE^{14,30}, F. FERRINI²³, F. FIDECARO^{14,30}, L. S. FINN⁸¹, I. FIORI²³, R. FISHER²⁴, R. FLAMINIO⁴², E. FOLEY¹⁸, S. FOLEY¹⁰, E. FORST⁶, N. FOTOPoulos¹, J.-D. FOURNIER⁴⁰, S. FRANCO³⁷, S. FRASCA^{19,68}, F. FRASCONI¹⁴, M. FREDE⁸, M. FREI⁵⁸, Z. FREI⁸², A. FREISE²⁰, R. FREY⁴⁷, T. T. FRICKE⁸, P. FRITSCHEL¹⁰, V. V. FROLOV⁶, M.-K. FUJIMOTO⁸³, P. FULDA¹⁶, M. FYFFE⁶, J. GAIR⁷¹, L. GAMMAITONI^{44,84}, J. GARCIA²⁵, F. GARUFI^{4,54}, N. GEHRELS³⁸, G. GEMME³², E. GENIN²³, A. GENNAI¹⁴, L. GERGELY⁸², S. GHOSH⁴³, J. A. GIAIME^{2,6}, S. GIAMPANIS¹², K. D. GIARDINA⁶, A. GIAZOTTO¹⁴, S. GIL-CASANOVA⁵³, C. GILL²⁶, J. GLEASON¹⁶, E. GOETZ⁸, R. GOETZ¹⁶, L. GONDAN⁸², G. GONZÁLEZ², N. GORDON²⁶, M. L. GORODETSKY³⁶, S. GOSSAN⁶², S. GOßLER⁸, R. GOUATY³, C. GRAEF⁸, P. B. GRAFF³⁸, M. GRANATA⁴², A. GRANT²⁶, S. GRAS¹⁰, C. GRAY²⁵, R. J. S. GREENHALGH⁸⁵, A. M. GRETARSSON⁸⁶, C. GRIFFO¹⁸, P. GROOT⁸⁷, H. GROTE⁸, K. GROVER²⁰, S. GRUNEWALD²¹, G. M. GUIDI^{45,46}, C. GUIDO⁶, K. E. GUSHWA¹, E. K. GUSTAFSON¹, R. GUSTAFSON⁵⁷, B. HALL⁴³, E. HALL¹, D. HAMMER¹², G. HAMMOND²⁶, M. HANKE⁸, J. HANKS²⁵, C. HANNA⁸⁸, J. HANSON⁶, J. HARMS¹, G. M. HARRY⁸⁹, I. W. HARRY²⁴, E. D. HARSTAD⁴⁷, M. T. HARTMAN¹⁶, K. HAUGHIAN²⁶, K. HAYAMA⁸³, J. HEEFNER^{1,142}, A. HEIDMANN⁴⁸, M. HEINTZE^{6,16}, H. HEITMANN⁴⁰, P. HELLO³⁷, G. HEMMING²³, M. HENDRY²⁶, I. S. HENG²⁶, A. W. HEPTONSTALL¹, M. HEURS⁸, S. HILD²⁶, D. HOAK⁵², K. A. HODGE¹, K. HOLT⁶, M. HOLTROP⁹⁰, T. HONG⁶², S. HOOPER³⁹, T. HORROM⁹¹, D. J. HOSKEN⁹², J. HOUGH²⁶, E. J. HOWELL³⁹, Y. HU²⁶, Z. HUA⁵⁶, V. HUANG⁶⁰, E. A. HUERTA²⁴, B. HUGHEY⁸⁶, S. HUSA⁵³, S. H. HUTTNER²⁶, M. HUYNH¹², T. HUYNH-DINH⁶, J. IAFRATE², D. R. INGRAM²⁵, R. INTA⁶⁴, T. ISOGAI¹⁰, A. IVANOV¹, B. R. IYER⁹³, K. IZUMI²⁵, M. JACOBSON¹, E. JAMES¹, H. JANG⁹⁴, Y. J. JANG⁹, P. JARANOWSKI⁹⁵, F. JIMÉNEZ-FORTEZA⁵³, W. W. JOHNSON², D. JONES²⁵, D. I. JONES⁹⁶, R. JONES²⁶, R. J. G. JONKER⁹, L. JU³⁹, HARIS K⁹⁷, P. KALMUS¹, V. KALOGERA⁷⁹, S. KANDHASAMY⁷², G. KANG⁹⁴, J. B. KANNER³⁸, M. KASPRZACK^{23,37}, R. KASTURI⁹⁸, E. KATSAVOUNIDIS¹⁰, W. KATZMAN⁶, H. KAUFER¹³, K. KAUFMAN⁶², K. KAWABE²⁵, S. KAWAMURA⁸³, F. KAWAZOE⁸, F. KÉFÉLIAN⁴⁰, D. KEITEL⁸, D. B. KELLEY²⁴, W. KELLS¹, D. G. KEPPEL⁸, A. KHALAIDOVSKI⁸, F. Y. KHALILI³⁶, E. A. KHAZANOV⁹⁹, B. K. KIM⁹⁴, C. KIM^{94,100}, K. KIM¹⁰¹, N. KIM²⁹, W. KIM⁹², Y.-M. KIM⁶³, E. J. KING⁹², P. J. KING¹, D. L. KINZEL⁶, J. S. KISSEL¹⁰, S. KLIMENKO¹⁶, J. KLINE¹², S. KOEHLLENBECK⁸, K. KOKEYAMA², V. KONDRASHOV¹, S. KORANDA¹², W. Z. KORTH¹, I. KOWALSKA⁴⁹, D. KOZAK¹, A. KREMIN⁷², V. KRINGEL⁸, B. KRISHNAN⁸, A. KRÓLAK^{102,103}, C. KUCHARCZYK²⁹, S. KUDLA², G. KUEHN⁸, A. KUMAR¹⁰⁴, P. KUMAR²⁴, R. KUMAR²⁶, R. KURDYUMOV²⁹, P. KWEE¹⁰, M. LANDRY²⁵, B. LANTZ²⁹, S. LARSON¹⁰⁵, P. D. LASKY¹⁰⁶, C. LAWRIE²⁶, A. LAZZARINI¹, A. LE ROUX⁶, P. LEACI²¹, E. O. LEBIGOT⁵⁶, C.-H. LEE⁶³, H. K. LEE¹⁰¹,

H. M. LEE¹⁰⁰, J. LEE¹⁰, J. LEE¹⁸, M. LEONARDI^{76,77}, J. R. LEONG⁸, N. LEROY³⁷, N. LETENDRE³, B. LEVINE²⁵, J. B. LEWIS¹, V. LHUILLIER²⁵, T. G. F. LI⁹, A. C. LIN²⁹, T. B. LITTENBERG⁷⁹, V. LITVINE¹, F. LIU¹⁰⁷, H. LIU⁷, Y. LIU⁵⁶, Z. LIU¹⁶, D. LLOYD¹, N. A. LOCKERBIE¹⁰⁸, V. LOCKETT¹⁸, D. LODHIA²⁰, K. LOEW⁸⁶, J. LOGUE²⁶, A. L. LOMBARDI⁵², M. LORENZINI⁵⁹, V. LORIETTE¹⁰⁹, M. LORMAND⁶, G. LOSURDO⁴⁵, J. LOUGH²⁴, J. LUAN⁶², M. J. LUBINSKI²⁵, H. LÜCK^{8,13}, A. P. LUNDGREN⁸, J. MACARTHUR²⁶, E. MACDONALD⁷, B. MACHENSCHALK⁸, M. MACINNIS¹⁰, D. M. MACLEOD⁷, F. MAGANA-SANDOVAL¹⁸, M. MAGESWARAN¹, K. MAILAND¹, E. MAJORANA¹⁹, I. MAKSIMOVIC¹⁰⁹, V. MALVEZZI⁵⁹, N. MAN⁴⁰, G. M. MANCA⁸, I. MANDEL²⁰, V. MANDIC⁷², V. MANGANO^{19,68}, M. MANTOVANI¹⁴, F. MARCHESONI^{44,110}, F. MARION³, S. MÁRKA²⁸, Z. MÁRKA²⁸, A. MARKOSYAN²⁹, E. MAROS¹, J. MARQUE²³, F. MARTELLI^{45,46}, I. W. MARTIN²⁶, R. M. MARTIN¹⁶, L. MARTINELLI⁴⁰, D. MARTYNOV¹, J. N. MARX¹, K. MASON¹⁰, A. MASSEROT³, T. J. MASSINGER²⁴, F. MATICHARD¹⁰, L. MATONE²⁸, R. A. MATZNER¹¹¹, N. MAVALVALA¹⁰, G. MAY², N. MAZUMDER⁹⁷, G. MAZZOLO⁸, R. MCCARTHY²⁵, D. E. MCCLELLAND⁶⁴, S. C. MCGUIRE¹¹², G. MCINTYRE¹, J. MCIVER⁵², D. MEACHER⁴⁰, G. D. MEADORS⁵⁷, M. MEHMET⁸, J. MEIDAM⁹, T. MEIER¹³, A. MELATOS¹⁰⁶, G. MENDELL²⁵, R. A. MERCER¹², S. MESHKOV¹, C. MESSENGER²⁶, M. S. MEYER⁶, H. MIAO⁶², C. MICHEL⁴², E. E. MIKHAILOV⁹¹, L. MILANO^{4,54}, J. MILLER⁶⁴, Y. MINENKOV⁵⁹, C. M. F. MINGARELLI²⁰, S. MITRA⁷⁵, V. P. MITROFANOV³⁶, G. MITSSELMAKHER¹⁶, R. MITTLEMAN¹⁰, B. MOE¹², M. MOHAN²³, S. R. P. MOHAPATRA^{24,58}, F. MOKLER⁸, D. MORARU²⁵, G. MORENO²⁵, N. MORGADO⁴², T. MORI⁸³, S. R. MORRIS³⁴, K. MOSSAVI⁸, B. MOURS³, C. M. MOW-LOWRY⁸, C. L. MUELLER¹⁶, G. MUELLER¹⁶, S. MUKHERJEE³⁴, A. MULLAVEY², J. MUNCH⁹², D. MURPHY²⁸, P. G. MURRAY²⁶, A. MYTIDIS¹⁶, M. F. NAGY⁷⁴, D. NANDA KUMAR¹⁶, I. NARDECCHIA^{19,68}, T. NASH¹, L. NATICCHIONI^{19,68}, R. NAYAK¹¹³, V. NECLA¹⁶, G. NELEMANS^{9,87}, I. NERI^{44,84}, M. NERI^{32,33}, G. NEWTON²⁶, T. NGUYEN⁶⁴, E. NISHIDA⁸³, A. NISHIZAWA⁸³, A. NITZ²⁴, F. NOCERA²³, D. NOLTING⁶, M. E. NORMANDIN³⁴, L. K. NUTTALL⁷, E. OCHSNER¹², J. O'DELL⁸⁵, E. OELKER¹⁰, G. H. OGIN¹, J. J. OH¹¹⁴, S. H. OH¹¹⁴, F. OHME⁷, P. OPPERMAN⁸, B. O'REILLY⁶, W. ORTEGA LARCHER³⁴, R. O'SHAUGHNESSY¹², C. OSTHELDER¹, D. J. OTTAWAY⁹², R. S. OTTENS¹⁶, J. OU⁶⁰, H. OVERMIER⁶, B. J. OWEN⁸¹, C. PADILLA¹⁸, A. PAI⁹⁷, C. PALOMBA¹⁹, Y. PAN⁵¹, C. PANKOW¹², F. PAOLETTI^{14,23}, R. PAOLETTI^{14,15}, M. A. PAPA^{12,21}, H. PARIS²⁵, A. PASQUALETTI²³, R. PASSAQUIETI^{14,30}, D. PASSUELLO¹⁴, M. PEDRAZA¹, P. PEIRIS⁵⁸, S. PENN⁹⁸, A. PERRECA²⁴, M. PHELPS¹, M. PICHOT⁴⁰, M. PICKENPACK⁸, F. PIERGIOVANNI^{45,46}, V. PIERRO⁶⁹, L. PINARD⁴², B. PINDOR¹⁰⁶, I. M. PINTO⁶⁹, M. PITKIN²⁶, J. POELD⁸, R. POGGIANI^{14,30}, V. POOLE⁴³, C. POUX¹, V. PREDOI⁷, T. PRESTEGARD⁷², L. R. PRICE¹, M. PRIJATELJ⁸, M. PRINCIPE⁶⁹, S. PRIVITERA¹, R. PRIX⁸, G. A. PRODI^{76,77}, L. PROKHOROV³⁶, O. PUNCKEN³⁴, M. PUNTURO⁴⁴, P. PUPPO¹⁹, V. QUETSCHKE³⁴, E. QUINTERO¹, R. QUITZOW-JAMES⁴⁷, F. J. RAAB²⁵, D. S. RABELING^{9,50}, I. RÁCZ⁷⁴, H. RADKINS²⁵, P. RAFFAI^{28,82}, S. RAJA¹¹⁵, G. RAJALAKSHMI¹¹⁶, M. RAKHMANOV³⁴, C. RAMET⁶, P. RAPAGNANI^{19,68}, V. RAYMOND¹, V. RE^{59,67}, C. M. REED²⁵, T. REED¹¹⁷, T. REGIMBAU⁴⁰, S. REID¹¹⁸, D. H. REITZE^{1,16}, F. RICCI^{19,68}, R. RIESEN⁶, K. RILES⁵⁷, N. A. ROBERTSON^{1,26}, F. ROBINET³⁷, A. ROCCHI⁵⁹, S. RODDY⁶, C. RODRIGUEZ⁷⁹, M. RODRUCK²⁵, C. ROEVER⁸, L. ROLLAND³, J. G. ROLLINS¹, J. D. ROMANO³⁴, R. ROMANO^{4,5}, G. ROMANOV⁹¹, J. H. ROMIE⁶, D. ROSIŃSKA^{31,119}, S. ROWAN²⁶, A. RÜDIGER⁸, P. RUGGI²³, K. RYAN²⁵, F. SALEMI⁸, L. SAMMUT¹⁰⁶, V. SANDBERG²⁵, J. SANDERS⁵⁷, V. SANNIBALE¹, I. SANTIAGO-PRIETO²⁶, E. SARACCO⁴², B. SASSOLAS⁴², B. S. SATHYAPRAKASH⁷, P. R. SAULSON²⁴, R. SAVAGE²⁵, R. SCHILLING⁸, R. SCHNABEL^{8,13}, R. M. S. SCHOFIELD⁴⁷, E. SCHREIBER⁸, D. SCHUETTE⁸, B. SCHULZ⁸, B. F. SCHUTZ^{7,21}, P. SCHWINBERG²⁵, J. SCOTT²⁶, S. M. SCOTT⁶⁴, F. SEIFERT¹, D. SELLERS⁶, A. S. SENGUPTA¹²⁰, D. SENTENAC²³, A. SERGEEV⁹⁹, D. SHADDOCK⁶⁴, S. SHAH^{9,87}, M. S. SHAHRIAR⁷⁹, M. SHALTEV⁸, B. SHAPIRO²⁹, P. SHAWHAN⁵¹, D. H. SHOEMAKER¹⁰, T. L. SIDERY²⁰, K. SIELEZ⁴⁰, X. SIEMENS¹², D. SIGG²⁵, D. SIMAKOV⁸, A. SINGER¹, L. SINGER¹, A. M. SINTES⁵³, G. R. SKELTON¹², B. J. J. SLAGMOLEN⁶⁴, J. SLUTSKY⁸, J. R. SMITH¹⁸, M. R. SMITH¹, R. J. E. SMITH²⁰, N. D. SMITH-LEFEBVRE¹, K. SODEN¹², E. J. SON¹¹⁴, B. SORAZU²⁶, T. SOURADEEP⁷⁵, L. SPERANDIO^{59,67}, A. STALEY²⁸, E. STEINERT²⁵, J. STEINLECHNER⁸, S. STEINLECHNER⁸, S. STEPLEWSKI⁴³, D. STEVENS⁷⁹, A. STOCHINO⁶⁴, R. STONE³⁴, K. A. STRAIN²⁶, N. STRANIERO⁴², S. STRIGIN³⁶, A. S. STROEER³⁴, R. STURANI^{45,46}, A. L. STUVER⁶, T. Z. SUMMERSCALES¹²¹, S. SUSMITHAN³⁹, P. J. SUTTON⁷, B. SWINKELS²³, G. SZEIFERT⁸², M. TACCA²⁷, D. TALUKDER⁴⁷, L. TANG³⁴, D. B. TANNER¹⁶, S. P. TARABRIN⁸, R. TAYLOR¹, A. P. M. TER BRAACK⁹, M. P. THIRUGNANASAMBANDAM¹, M. THOMAS⁶, P. THOMAS²⁵, K. A. THORNE⁶, K. S. THORNE⁶², E. THRANE¹, V. TIWARI¹⁶, K. V. TOKMAKOV¹⁰⁸, C. TOMLINSON⁷³, A. TONCELLI^{14,30}, M. TONELLI^{14,30}, O. TORRE^{14,15}, C. V. TORRES³⁴, C. I. TORRIE^{1,26}, F. TRAVASSO^{44,84}, G. TRAYLOR⁶, M. TSE²⁸, D. UGOLINI¹²², C. S. UNNIKRISHNAN¹¹⁶, H. VAHLBRUCH¹³, G. VAJENTE^{14,30}, M. VALLISNERI⁶², J. F. J. VAN DEN BRAND^{9,50}, C. VAN DEN BROECK⁹, S. VAN DER PUTTEN⁹, M. V. VAN DER SLUYS^{9,87}, J. VAN HEIJNINGEN⁹, A. A. VAN VEGGEL²⁶, S. VASS¹, M. VASÚTH⁷⁴, R. VAULIN¹⁰, A. VECCHIO²⁰, G. VEDOVATO¹²³, J. VEITCH⁹, P. J. VEITCH⁹², K. VENKATESWARA¹²⁴, D. VERKINDT³, S. VERMA³⁹, F. VETRANO^{45,46}, A. VICERÉ^{45,46}, R. VINCENT-FINLEY¹¹², J.-Y. VINET⁴⁰, S. VITALE^{9,10}, B. VLCEK¹², T. VO²⁵, H. VOCCA^{44,84}, C. VORVICK²⁵, W. D. VOUSDEN²⁰, D. VRINCEANU³⁴, S. P. VYACHANIN³⁶, A. WADE⁶⁴, L. WADE¹², M. WADE¹², S. J. WALDMAN¹⁰, M. WALKER², L. WALLACE¹, Y. WAN⁵⁶, J. WANG⁶⁰, M. WANG²⁰, X. WANG⁵⁶, A. WANNER⁸, R. L. WARD⁶⁴, M. WAS⁸, B. WEAVER²⁵, L.-W. WEI⁴⁰, M. WEINERT⁸, A. J. WEINSTEIN¹, R. WEISS¹⁰, T. WELBORN⁶, L. WEN³⁹, P. WESSELS⁸, M. WEST²⁴, T. WESTPHAL⁸, K. WETTE⁸, J. T. WHELAN⁵⁸, S. E. WHITCOMB^{1,39}, D. J. WHITE⁷³, B. F. WHITING¹⁶, S. WIBOWO¹², K. WIESNER⁸, C. WILKINSON²⁵, L. WILLIAMS¹⁶, R. WILLIAMS¹, T. WILLIAMS¹²⁵, J. L. WILLIS¹²⁶, B. WILLKE^{8,13}, M. WIMMER⁸, L. WINKELMANN⁸, W. WINKLER⁸, C. C. WIPP¹⁰, H. WITTEL⁸, G. WOAN²⁶, J. WORDEN²⁵, J. YABLON⁷⁹, I. YAKUSHIN⁶, H. YAMAMOTO¹, C. C. YANCEY⁵¹, H. YANG⁶², D. YEATON-MASSEY¹, S. YOSHIDA¹²⁵, H. YUM⁷⁹, M. YVERT³, A. ZADROŻNY¹⁰³, M. ZANOLIN⁸⁶, J.-P. ZENDRI¹²³, F. ZHANG¹⁰, L. ZHANG¹, C. ZHAO³⁹, H. ZHU⁸¹, X. J. ZHU³⁹, N. ZOTOV^{117,143}, M. E. ZUCKER¹⁰, AND J. ZWEIZIG¹

THE LIGO SCIENTIFIC COLLABORATION & THE VIRGO COLLABORATION

AND

S. BUCHNER^{127,128}, I. COGNARD^{129,130}, A. CORONGIU¹³¹, N. D'AMICO^{131,132}, C. M. ESPINOZA^{133,134}, P. C. C. FREIRE¹³⁵,
 E. V. GOTTHELF²⁸, L. GUILLEMOT¹³⁵, J. W. T. HESSELS^{136,137}, G. B. HOBBS¹³⁸, M. KRAMER^{133,135}, A. G. LYNE¹³³,
 F. E. MARSHALL³⁷, A. POSSENTI¹³¹, S. M. RANSOM¹³⁹, P. S. RAY¹⁴⁰, J. ROY¹⁴¹, AND B. W. STAPPERS¹³³

¹ LIGO - California Institute of Technology, Pasadena, CA 91125, USA

² Louisiana State University, Baton Rouge, LA 70803, USA

³ Laboratoire d'Annecy-le-Vieux de Physique des Particules (LAPP), Université de Savoie, CNRS/IN2P3, F-74941 Annecy-le-Vieux, France

⁴ INFN, Sezione di Napoli, Complesso Universitario di Monte S. Angelo, I-80126 Napoli, Italy

⁵ Università di Salerno, Fisciano, I-84084 Salerno, Italy

⁶ LIGO - Livingston Observatory, Livingston, LA 70754, USA

⁷ Cardiff University, Cardiff, CF24 3AA, UK

⁸ Albert-Einstein-Institut, Max-Planck-Institut für Gravitationsphysik, D-30167 Hannover, Germany

⁹ Nikhef, Science Park, 1098 XG Amsterdam, The Netherlands

¹⁰ LIGO - Massachusetts Institute of Technology, Cambridge, MA 02139, USA

¹¹ Instituto Nacional de Pesquisas Espaciais, 12227-010 - São José dos Campos, SP, Brazil

¹² University of Wisconsin-Milwaukee, Milwaukee, WI 53201, USA

¹³ Leibniz Universität Hannover, D-30167 Hannover, Germany

¹⁴ INFN, Sezione di Pisa, I-56127 Pisa, Italy

¹⁵ Università di Siena, I-53100 Siena, Italy

¹⁶ University of Florida, Gainesville, FL 32611, USA

¹⁷ The University of Mississippi, University, MS 38677, USA

¹⁸ California State University Fullerton, Fullerton, CA 92831, USA

¹⁹ INFN, Sezione di Roma, I-00185 Roma, Italy

²⁰ University of Birmingham, Birmingham, B15 2TT, UK

²¹ Albert-Einstein-Institut, Max-Planck-Institut für Gravitationsphysik, D-14476 Golm, Germany

²² Montana State University, Bozeman, MT 59717, USA

²³ European Gravitational Observatory (EGO), I-56021 Cascina, Pisa, Italy

²⁴ Syracuse University, Syracuse, NY 13244, USA

²⁵ LIGO - Hanford Observatory, Richland, WA 99352, USA

²⁶ SUPA, University of Glasgow, Glasgow, G12 8QQ, UK

²⁷ APC, AstroParticule et Cosmologie, Université Paris Diderot, CNRS/IN2P3, CEA/Irfu, Observatoire de Paris, Sorbonne Paris Cité,

10, rue Alice Domon et Léonie Duquet, F-75205 Paris Cedex 13, France

²⁸ Columbia University, New York, NY 10027, USA

²⁹ Stanford University, Stanford, CA 94305, USA

³⁰ Università di Pisa, I-56127 Pisa, Italy

³¹ CAMK-PAN, 00-716 Warsaw, Poland

³² INFN, Sezione di Genova, I-16146 Genova, Italy

³³ Università degli Studi di Genova, I-16146 Genova, Italy

³⁴ The University of Texas at Brownsville, Brownsville, TX 78520, USA

³⁵ San Jose State University, San Jose, CA 95192, USA

³⁶ Moscow State University, Moscow 119992, Russia

³⁷ LAL, Université Paris-Sud, IN2P3/CNRS, F-91898 Orsay, France

³⁸ NASA/Goddard Space Flight Center, Greenbelt, MD 20771, USA

³⁹ University of Western Australia, Crawley, WA 6009, Australia

⁴⁰ Université Nice-Sophia-Antipolis, CNRS, Observatoire de la Côte d'Azur, F-06304 Nice, France

⁴¹ Institut de Physique de Rennes, CNRS, Université de Rennes 1, F-35042 Rennes, France

⁴² Laboratoire des Matériaux Avancés (LMA), IN2P3/CNRS, Université de Lyon, F-69622 Villeurbanne, Lyon, France

⁴³ Washington State University, Pullman, WA 99164, USA

⁴⁴ INFN, Sezione di Perugia, I-06123 Perugia, Italy

⁴⁵ INFN, Sezione di Firenze, I-50019 Sesto Fiorentino, Firenze, Italy

⁴⁶ Università degli Studi di Urbino "Carlo Bo," I-61029 Urbino, Italy

⁴⁷ University of Oregon, Eugene, OR 97403, USA

⁴⁸ Laboratoire Kastler Brossel, ENS, CNRS, UPMC, Université Pierre et Marie Curie, F-75005 Paris, France

⁴⁹ Astronomical Observatory Warsaw University, 00-478 Warsaw, Poland

⁵⁰ VU University Amsterdam, 1081 HV Amsterdam, The Netherlands

⁵¹ University of Maryland, College Park, MD 20742, USA

⁵² University of Massachusetts - Amherst, Amherst, MA 01003, USA

⁵³ Universitat de les Illes Balears, E-07122 Palma de Mallorca, Spain

⁵⁴ Università di Napoli "Federico II," Complesso Universitario di Monte S. Angelo, I-80126 Napoli, Italy

⁵⁵ Canadian Institute for Theoretical Astrophysics, University of Toronto, Toronto, Ontario, M5S 3H8, Canada

⁵⁶ Tsinghua University, Beijing 100084, China

⁵⁷ University of Michigan, Ann Arbor, MI 48109, USA

⁵⁸ Rochester Institute of Technology, Rochester, NY 14623, USA

⁵⁹ INFN, Sezione di Roma Tor Vergata, I-00133 Roma, Italy

⁶⁰ National Tsing Hua University, Hsinchu 300, Taiwan

⁶¹ Charles Sturt University, Wagga Wagga, NSW 2678, Australia

⁶² Caltech-CaRT, Pasadena, CA 91125, USA

⁶³ Pusan National University, Busan 609-735, Korea

⁶⁴ Australian National University, Canberra, ACT 0200, Australia

⁶⁵ Carleton College, Northfield, MN 55057, USA

⁶⁶ INFN, Gran Sasso Science Institute, I-67100 L'Aquila, Italy

⁶⁷ Università di Roma Tor Vergata, I-00133 Roma, Italy

⁶⁸ Università di Roma "La Sapienza," I-00185 Roma, Italy

⁶⁹ University of Sannio at Benevento, I-82100 Benevento, Italy and INFN (Sezione di Napoli), Italy

⁷⁰ The George Washington University, Washington, DC 20052, USA

⁷¹ University of Cambridge, Cambridge, CB2 1TN, UK

⁷² University of Minnesota, Minneapolis, MN 55455, USA

- ⁷³ The University of Sheffield, Sheffield S10 2TN, UK
- ⁷⁴ Wigner RCP, RMKI, H-1121 Budapest, Konkoly Thege Miklós út 29-33, Hungary
- ⁷⁵ Inter-University Centre for Astronomy and Astrophysics, Pune - 411007, India
- ⁷⁶ INFN, Gruppo Collegato di Trento, I-38050 Povo, Trento, Italy
- ⁷⁷ Università di Trento, I-38050 Povo, Trento, Italy
- ⁷⁸ California Institute of Technology, Pasadena, CA 91125, USA
- ⁷⁹ Northwestern University, Evanston, IL 60208, USA
- ⁸⁰ Montclair State University, Montclair, NJ 07043, USA
- ⁸¹ The Pennsylvania State University, University Park, PA 16802, USA
- ⁸² MTA-Eotvos University, 'Lendulet' A. R. G., Budapest 1117, Hungary
- ⁸³ National Astronomical Observatory of Japan, Tokyo 181-8588, Japan
- ⁸⁴ Università di Perugia, I-06123 Perugia, Italy
- ⁸⁵ Rutherford Appleton Laboratory, HSI, Chilton, Didcot, Oxon, OX11 0QX, UK
- ⁸⁶ Embry-Riddle Aeronautical University, Prescott, AZ 86301, USA
- ⁸⁷ Department of Astrophysics/IMAPP, Radboud University Nijmegen, P.O. Box 9010, 6500 GL Nijmegen, The Netherlands
- ⁸⁸ Perimeter Institute for Theoretical Physics, Ontario, N2L 2Y5, Canada
- ⁸⁹ American University, Washington, DC 20016, USA
- ⁹⁰ University of New Hampshire, Durham, NH 03824, USA
- ⁹¹ College of William and Mary, Williamsburg, VA 23187, USA
- ⁹² University of Adelaide, Adelaide, SA 5005, Australia
- ⁹³ Raman Research Institute, Bangalore, Karnataka 560080, India
- ⁹⁴ Korea Institute of Science and Technology Information, Daejeon 305-806, Korea
- ⁹⁵ Białystok University, 15-424 Białystok, Poland
- ⁹⁶ University of Southampton, Southampton, SO17 1BJ, UK
- ⁹⁷ IISER-TVM, CET Campus, Trivandrum Kerala 695016, India
- ⁹⁸ Hobart and William Smith Colleges, Geneva, NY 14456, USA
- ⁹⁹ Institute of Applied Physics, Nizhny Novgorod, 603950, Russia
- ¹⁰⁰ Seoul National University, Seoul 151-742, Korea
- ¹⁰¹ Hanyang University, Seoul 133-791, Korea
- ¹⁰² IM-PAN, 00-956 Warsaw, Poland
- ¹⁰³ NCBJ, 05-400 Świerk-Otwock, Poland
- ¹⁰⁴ Institute for Plasma Research, Bhat, Gandhinagar 382428, India
- ¹⁰⁵ Utah State University, Logan, UT 84322, USA
- ¹⁰⁶ The University of Melbourne, Parkville, VIC 3010, Australia
- ¹⁰⁷ University of Brussels, Brussels 1050 Belgium
- ¹⁰⁸ SUPA, University of Strathclyde, Glasgow, G1 1XQ, UK
- ¹⁰⁹ ESPCI, CNRS, F-75005 Paris, France
- ¹¹⁰ Università di Camerino, Dipartimento di Fisica, I-62032 Camerino, Italy
- ¹¹¹ The University of Texas at Austin, Austin, TX 78712, USA
- ¹¹² Southern University and A&M College, Baton Rouge, LA 70813, USA
- ¹¹³ IISER-Kolkata, Mohanpur, West Bengal 741252, India
- ¹¹⁴ National Institute for Mathematical Sciences, Daejeon 305-390, Korea
- ¹¹⁵ RRCAT, Indore MP 452013, India
- ¹¹⁶ Tata Institute for Fundamental Research, Mumbai 400005, India
- ¹¹⁷ Louisiana Tech University, Ruston, LA 71272, USA
- ¹¹⁸ SUPA, University of the West of Scotland, Paisley, PA1 2BE, UK
- ¹¹⁹ Institute of Astronomy, 65-265 Zielona Góra, Poland
- ¹²⁰ Indian Institute of Technology, Gandhinagar Ahmedabad Gujarat 382424, India
- ¹²¹ Andrews University, Berrien Springs, MI 49104, USA
- ¹²² Trinity University, San Antonio, TX 78212, USA
- ¹²³ INFN, Sezione di Padova, I-35131 Padova, Italy
- ¹²⁴ University of Washington, Seattle, WA 98195, USA
- ¹²⁵ Southeastern Louisiana University, Hammond, LA 70402, USA
- ¹²⁶ Abilene Christian University, Abilene, TX 79699, USA
- ¹²⁷ Hartebeesthoek Radio Astronomy Observatory, PO Box 443, Krugersdorp 1740, South Africa
- ¹²⁸ School of Physics, University of the Witwatersrand, Johannesburg, South Africa
- ¹²⁹ LPC2E/CNRS-Université d'Orléans, F-45071 Orléans, France
- ¹³⁰ Nançay/Paris Observatory, F-18330 Nançay, France
- ¹³¹ INAF - Osservatorio Astronomico di Cagliari, Poggio dei Pini, I-09012 Capoterra, Italy
- ¹³² Dipartimento di Fisica Università di Cagliari, Cittadella Universitaria, I-09042 Monserrato, Italy
- ¹³³ Jodrell Bank Centre for Astrophysics, School of Physics and Astronomy, University of Manchester, Manchester M13 9PL, UK
- ¹³⁴ Instituto de Astrofísica, Facultad de Física, Pontificia Universidad Católica de Chile, Casilla 306, Santiago 22, Chile
- ¹³⁵ Max-Planck-Institut für Radioastronomie, Auf dem Hügel 69, D-53121 Bonn, Germany
- ¹³⁶ ASTRON, the Netherlands Institute for Radio Astronomy, Postbus 2, 7990 AA, Dwingeloo, The Netherlands
- ¹³⁷ Astronomical Institute "Anton Pannekoek," University of Amsterdam, Science Park 904, 1098 XH Amsterdam, The Netherlands
- ¹³⁸ Australia Telescope National Facility, CSIRO, P.O. Box 76, Epping NSW 1710, Australia
- ¹³⁹ National Radio Astronomy Observatory, Charlottesville, VA 22903, USA
- ¹⁴⁰ Space Science Division, Naval Research Laboratory, Washington, DC 20375-5352, USA
- ¹⁴¹ National Centre for Radio Astrophysics, Pune 411007, India

Received 2013 September 30; accepted 2014 February 28; published 2014 April 2

ABSTRACT

We present the results of searches for gravitational waves from a large selection of pulsars using data from the most recent science runs (S6, VSR2 and VSR4) of the initial generation of interferometric gravitational wave detectors LIGO (Laser Interferometric Gravitational-wave Observatory) and Virgo. We do not see evidence for gravitational wave emission from any of the targeted sources but produce upper limits on the emission amplitude. We highlight the results from seven young pulsars with large spin-down luminosities. We reach within a factor of five of the canonical spin-down limit for all seven of these, whilst for the Crab and Vela pulsars we further surpass their spin-down limits. We present new or updated limits for 172 other pulsars (including both young and millisecond pulsars). Now that the detectors are undergoing major upgrades, and, for completeness, we bring together all of the most up-to-date results from all pulsars searched for during the operations of the first-generation LIGO, Virgo and GEO600 detectors. This gives a total of 195 pulsars including the most recent results described in this paper.

Key words: gravitational waves – pulsars: general

Online-only material: color figures

1. INTRODUCTION

Pulsars are spinning, magnetized neutron stars with slowly decreasing rotation rates. In the model of a triaxial ellipsoid star, a deformation (possibly from shear strains in the solid part(s) of the star, or from magnetic stresses) can appear as a time-varying quadrupole moment as the star rotates. The observed loss of rotational energy, known as the spin-down luminosity (given by $\dot{E} = I_{zz}\Omega|\dot{\Omega}| = 4\pi^2 I_{zz} f_{\text{rot}} |\dot{f}_{\text{rot}}|$, where I_{zz} is the moment of inertia around the principal axis (aligned with the rotation axis), f_{rot} is the rotation frequency, and \dot{f}_{rot} is the rotational frequency derivative) provides a huge reservoir of energy. Along with magnetic dipole radiation some fraction of this reservoir is potentially dissipated through gravitational wave emission (see Shklovskii 1969; Ostriker & Gunn 1969; Ferrari & Ruffini 1969; Melosh 1969 for four contemporaneous calculations of gravitational wave emission from soon after pulsars were discovered, or e.g., Owen 2006 for a review of more recent emission mechanism calculations). Known pulsars usually have precisely determined frequency evolutions and sky-positions making them ideal targets for gravitational wave detectors. If a pulsar is monitored regularly through electromagnetic observations it can yield a coherent phase model, which allows gravitational wave data to be coherently integrated over months or years.

Since the initial science data runs of the Laser Interferometric Gravitational-wave Observatory (LIGO), Virgo and GEO600, searches have been performed for continuous quasi-monochromatic gravitational wave emission from many known pulsars (Abbott et al. 2004, 2005, 2007a, 2008, 2010; Abadie et al. 2011). Most recently 116 known pulsars were targeted using data from LIGO’s fifth science run (S5; Abbott et al. 2010), and the Vela pulsar (J0835–4510) was targeted using data from Virgo’s second science run (VSR2). These searches reported no detections, but provided upper limits on the gravitational wave amplitude from the sources and surpassed the so-called spin-down limit (see Section 1.1) for the Crab and Vela pulsars.

We aim here to search for gravitational wave emission from a large selection of stars including some of those with the largest spin-down luminosities. Due to the sensitivity reduction caused at low frequency by seismic noise at the detectors, it is not worthwhile to search for pulsars with rotational frequencies, f_{rot} , smaller than about 10 Hz, which corresponds to gravitational wave mass quadrupole emission at frequencies, $f_{\text{gw}} = 2f_{\text{rot}}$, smaller than 20 Hz. The exact value of this gravitational wave

low-frequency cut-off is rather arbitrary, our choice of taking 20 Hz is motivated by the presence of several noise lines and bumps in Virgo data at lower frequencies. In general, young pulsars, with large spin-down luminosities are searched for at lower frequencies where the Virgo detector has better sensitivity, whereas the search for millisecond pulsars (MSPs) is conducted at higher frequencies where the LIGO detectors are more sensitive. The selection of pulsars will be discussed more fully in Section 2.

1.1. The Signal

The expected quadrupolar gravitational wave signal from a triaxial neutron star¹⁴⁴ steadily spinning about one of its principal axes of inertia is at twice the rotation frequency, with a strain of

$$h(t) = \frac{1}{2} F_+(t, \psi) h_0 (1 + \cos^2 \iota) \cos \phi(t) + F_\times(t, \psi) h_0 \cos \iota \sin \phi(t) \quad (1)$$

in the detector, where

$$h_0 = \frac{16\pi^2 G}{c^4} \frac{I_{zz} \varepsilon f_{\text{rot}}^2}{d} \quad (2)$$

is the dimensionless gravitational wave strain amplitude. h_0 is dependent on I_{zz} , the fiducial equatorial ellipticity, defined as $\varepsilon = (I_{xx} - I_{yy})/I_{zz}$ in terms of principal moments of inertia, the rotational frequency, f_{rot} , and the distance to the source d . The signal amplitudes in the two polarizations (“+” and “×”) depend on the inclination of the star’s rotation axis to the line-of-sight, ι , while the detector antenna pattern responses for the two polarization states, $F_+(t, \psi)$ and $F_\times(t, \psi)$, depend on the gravitational wave polarization angle, ψ , as well as the detector location, orientation and source sky position. The gravitational wave phase evolution, $\phi(t)$, depends on both the intrinsic rotational frequency and frequency derivatives of the pulsar and on Doppler and propagation effects. These extrinsic effects include relativistic modulations caused by the Earth’s orbital and rotational motion, the presence of massive bodies in the solar system close to the line-of-sight to the pulsar, the proper motion of the pulsar, and (in the case of a binary system) pulsar orbital motions. We will assume that $\phi(t)$ is phase-locked to the electromagnetic pulse phase evolution, but with double

¹⁴² Deceased, 2012 April.

¹⁴³ Deceased, 2012 May.

¹⁴⁴ We use “triaxial neutron star” as shorthand for a star with some asymmetry with respect to its rotation axis and therefore a triaxial moment of inertia ellipsoid.

Table 1
Science Runs

| Run | Dates | Duty Factor (%) | Data Length (days) |
|--------------------|--|-----------------|--------------------|
| VSR2 | 2009 Jul 7 (20:55 UTC) – 2010 Jan 8 (22:00 UTC) | 80.4 | 149 |
| VSR4 | 2011 Jun 3 (10:27 UTC) – 2011 Sep 5 (13:26 UTC) | 81.0 | 76 |
| S6 Hanford (H1) | 2009 Jul 7 (21:00 UTC) – 2010 Oct 21 (00:00 UTC) | 50.6 | 238 |
| S6 Livingston (L1) | 2009 Jul 7 (21:00 UTC) – 2010 Oct 21 (00:00 UTC) | 47.9 | 225 |

the value and with an initial phase offset, ϕ_0 . Given this phase evolution, the four unknown search parameters are simply h_0 , $\cos \iota$, ϕ_0 and ψ . The gravitational wave amplitude is related to the star’s $l = m = 2$ mass quadrupole moment via (see, e.g., Owen 2005)

$$Q_{22} = \sqrt{\frac{15}{8\pi}} I_{zz} \varepsilon = h_0 \left(\frac{c^4 d}{16\pi^2 G f_{\text{rot}}^2} \right) \sqrt{\frac{15}{8\pi}}, \quad (3)$$

where Q_{22} is the slightly non-standard definition of quadrupole moment used in Ushomirsky et al. (2000) and many subsequent papers. This value can be constrained independently of any assumptions about the star’s equation of state and moment of inertia.

If we allocate all the spin-down luminosity, \dot{E} , to gravitational wave luminosity, \dot{E}_{gw} , where

$$\begin{aligned} \dot{E}_{\text{gw}} &= \frac{2048\pi^6 G}{5 c^5} f_{\text{rot}}^6 (I_{zz} \varepsilon)^2, \\ &= \frac{8\pi^2 c^3}{5 G} f_{\text{rot}}^2 h_0^2 d^2, \end{aligned} \quad (4)$$

then we have the canonical “spin-down limit” on gravitational wave strain¹⁴⁵

$$\begin{aligned} h_0^{\text{sd}} &= \left(\frac{5 G I_{zz} \dot{f}_{\text{rot}}}{2 c^3 d^2 f_{\text{rot}}} \right)^{1/2} \\ &= 8.06 \times 10^{-19} \frac{I_{38}^{1/2}}{d_{\text{kpc}}} \left(\frac{|\dot{f}_{\text{rot}}|}{f_{\text{rot}}} \right)^{1/2}, \end{aligned} \quad (5)$$

where I_{38} is the star’s moment of inertia in the units of 10^{38} kg m^2 , and d_{kpc} is the distance to the pulsar in kiloparsecs. The spin-down limit on the signal amplitude corresponds (via Equation (2)) to an upper limit on the star’s fiducial ellipticity¹⁴⁶

$$\varepsilon^{\text{sd}} = 0.237 \left(\frac{h_0^{\text{sd}}}{10^{-24}} \right) f_{\text{rot}}^{-2} I_{38}^{-1} d_{\text{kpc}}. \quad (6)$$

Johnson-McDaniel (2013) shows how to relate this to the physical ellipticity of the star’s surface for a given equation of state.

A gravitational wave strain upper limit that is below the spin-down limit is an important milestone, as such a measurement is probing uncharted regions of the parameter space. Likewise it directly constrains the fraction of spin-down power that could be due to the emission of gravitational waves, which gives insight into the overall spin-down energy budget.

¹⁴⁵ As noted in Johnson-McDaniel (2013), the versions of this equation given inline in the first paragraph of Abbott et al. (2008), as Equation (1) in Abbott et al. (2010) and as Equation (14) in Abadie et al. (2011) are incorrect and should have I_{38} substituted for $I_{38}^{1/2}$.

¹⁴⁶ Again, as noted in Johnson-McDaniel (2013), the versions of this equation given inline in Section 3 of Abbott et al. (2008) and as Equation (7) in Abbott et al. (2010) are incorrect and should have I_{38} substituted for I_{38}^{-1} .

1.2. The Science Runs

In this paper we have used calibrated data from the Virgo second (Aasi et al. 2012) and fourth science runs (VSR2 and VSR4) and the LIGO sixth science run (S6). Virgo’s third science run (VSR3) was relatively insensitive in comparison with VSR4 and has not been included in this analysis. This was partially because Virgo introduced monolithic mirror suspensions prior to VSR4 which improved sensitivity in the low-frequency range. During S6, the two LIGO 4 km detectors at Hanford, Washington (LHO/H1), and Livingston, Louisiana (LLO/L1), were running in an enhanced configuration (Adhikari et al. 2006) over that from the previous S5 run (Abbott et al. 2009). Table 1 shows dates of the runs, the duty factors and science data lengths for each detector that we analyzed.

The Virgo and LIGO data used in these analyses have been calibrated through different reconstruction procedures, but both based ultimately on the measured response to actuation controls on the positions of the mirrors that define the interferometers. For Virgo VSR2, the calibration uncertainty was about 5.5% in amplitude and $\sim 50 \text{ mrad}$ (3°) in phase over most of the frequency range (Accadia et al. 2011). For VSR4, the uncertainty amounted to about 7.5% in amplitude and to $(40 + 50f) \text{ mrad}$ in phase, where f is the frequency in kilohertz, for frequencies up to 500 Hz (Mours & Rolland 2011). For LIGO, the S6 calibration uncertainties over the relevant frequency range (50–1500 Hz) were up to $\sim 19\%$ in amplitude and $\sim 170 \text{ mrad}$ (10°) in phase for L1, and up to $\sim 16\%$ in amplitude and $\sim 120 \text{ mrad}$ (7°) for H1 (Bartos et al. 2011). These phase errors are well within the range (i.e., less than 30°) as applied in Abbott et al. (2007a) that would cause significant loss in signal power due to decoherence between the pulsar signal and the assumed phase evolution.

1.3. Methods

We used three semi-independent methods (very similar to those used in the Vela pulsar search in Abadie et al. 2011) to search for signals described in Section 1.1. Here, we briefly outline their operation, but for full descriptions we refer the reader to the references below. Two of the search methods work with time domain data that has been heterodyned to remove the signal’s phase evolution and then heavily decimated. This leaves a complex data stream in which any signal would only be modulated by the detector’s beam pattern. In the first method, this data stream is used to give Bayesian parameter estimates of the unknown signal parameters¹⁴⁷ (Dupuis & Woan 2005). The second method computes the maximum likelihood \mathcal{F} -statistic rather than a Bayesian posterior (or in case where ψ and ι

¹⁴⁷ For this analysis the parameter posterior distributions were recreated using a Markov chain Monte Carlo (Abbott et al. 2010). For each pulsar five independent chains were produced with 50,000 burn-in samples and 200,000 posterior samples in each. The chains were thinned using the autocorrelation length to give uncorrelated samples, and to test for convergence, the chains were then examined by eye, and a Gelman-Rubins test was performed (see, e.g., Brooks & Roberts 1998).

are well constrained, the \mathcal{G} -statistic) (Jaranowski & Królak 2010). The third method (Astone et al. 2010) makes use of a Short Fourier Transform Database (SFDB) of each detector’s data. After the extraction of a small frequency band around the signal’s expected frequency, the Doppler effect, Einstein delay and spin-down are removed in the time domain and the data are down-sampled with a re-sampling technique. Two matched filters on the “+” and “ \times ” signal Fourier components are then computed at the five frequencies at which the signal power is spread due to the signal amplitude and phase modulation; they are used to build a detection statistic and to estimate signal parameters in the case of detection. This 5-vector method has been extended over that used in Abadie et al. (2011) to allow for coherent analysis of data from multiple detectors (Astone et al. 2012). Each of these methods can incorporate prior information on the pulsar’s inclination and polarization angle. From here on, we will refer to the first method as the *Bayesian* method,¹⁴⁸ the second as the \mathcal{F}/\mathcal{G} -statistic method and the third as the *5n-vector* method, where n refers to the number of datasets coherently combined.

All three methods apply some data cleaning. The procedure used to obtain the heterodyned data removes extreme outliers by running two passes of a scheme that identifies points with absolute values greater than five times the standard deviation of the dataset. The \mathcal{F}/\mathcal{G} -statistic method performs further cleaning of this data through the Grubbs test (see Abadie et al. 2011). In the *5n-vector* method, after an initial time-domain cleaning before the construction of the SFDB, a further cleaning step is applied on the final down-sampled time series in which the largest outliers belonging to the non-Gaussian tail of the data amplitude distribution are removed.

We have incorporated some limits from the previous LIGO S5 results (Abbott et al. 2010) as priors in the Bayesian analysis. However, the S6/VSR2.4 phase models were produced with updated pulsar ephemerides resulting in an unknown phase offset between them and the S5 results. We have, therefore, simply used the S5 marginalized posterior on h_0 and $\cos \iota$, $p(h_0, \cos \iota)$, as our prior for the new results. In the case of glitching pulsars (see Section 2), we used the same approach and (incoherently) combined the separate coherent analyses produced between glitches. In the case of the \mathcal{F}/\mathcal{G} -statistic method, the results from different detectors or different inter-glitch periods are combined incoherently by adding the respective statistics. Also, for the *5n-vector* method, results from different inter-glitch periods are incoherently combined by summing the corresponding statistics. Our reasons for not coherently combining the data over glitches are twofold. The first is that we do not know how a glitch would effect the relative phase offset between the electromagnetic pulses and the gravitational wave signal. The second reason is a practical consideration based on the timing solutions we have for our pulsars. For three of the four glitching pulsars (all except J0537–6910) in this analysis we have separate timing solutions for each inter-glitch period. These separate timing solutions, as provided by the pulsar timing software TEMPO(2), do not give an epoch defined at a fixed pulse phase (i.e., the epoch is not given as the time of the peak of a particular pulse), so there is some unknown phase offset between the separate solutions. However, if this phase offset were known (e.g., by going back to the original pulsar pulse time of arrival data) the gain in sensitivity would still be minimal: for

the Vela pulsar and J1813–1246 the data from VSR4 (which was after the glitches in these pulsars) was much more sensitive, so completely dominates the result; for J1952+3252 the post-glitch data contains the latter part of S6, which was more sensitive and would again dominate the results. For J0537–6910 the epoch for each inter-glitch timing solution is defined (see Appendix), so the electromagnetic phase could be tracked over the glitches, but again our result is dominated by the longest and most sensitive inter-glitch period.

Even without a detection, all three methods can be used to produce upper limits on the gravitational wave amplitude from the pulsars. Here, we will quote 95% confidence upper limits on the amplitude. In the Bayesian method, an upper limit on the h_0 posterior (after marginalization over the orientation parameters) is found by calculating the upper bound, from zero, on the integral over this posterior that encloses 95% of the probability. In the \mathcal{F}/\mathcal{G} -statistic method, a frequentist upper limit is calculated through Monte-Carlo simulations, which find the value of h_0 for which 95% of trials exceed the maximum likelihood statistic.¹⁴⁹ The *5n-vector* method computes an upper limit on the H_0 posterior, given the actual value of the detection statistic, and the marginalization over the other parameters is implicitly done in the Monte Carlo simulation used to compute the likelihood. The amplitude, H_0 , is linked to the classical h_0 , given by Equation (2), by the relation $H_0 = (h_0/2)\sqrt{1 + 6 \cos^2 \iota + \cos^4 \iota}$ (see Equation (A5) in Abadie et al. 2011). H_0 is the strain amplitude of a linearly polarized signal with polarization angle $\psi = 0$. In order to convert an upper limit on H_0 to an upper limit on h_0 , we use the previous equation replacing the coefficient on the right hand side with its mean value over the distribution of $\cos \iota$ used in the upper limit procedure. This is justified by the fact that the posterior distribution of H_0 is not dependent on ι . The three methods have been tested with hardware and software simulated signal injections to check that they can recover the expected signal model (see, e.g., Abadie et al. 2011). In the Bayesian analysis these upper limits are really 95% credibility, or degrees-of-belief, values, whereas for the frequentist analysis these are 95% confidence values. These are both asking different questions and in general should not be expected to produce identical results. A brief discussion of this is given in the first search for a pulsar in LIGO data in Abbott et al. (2004), whilst a more technical discussion of the differences between the upper limits can be found in Röver et al. (2011).

2. PULSAR SELECTION

The sensitivity of the Virgo and LIGO detectors allows us to target pulsars with $f_{\text{rot}} > 10$ Hz. Currently the Australia Telescope National Facility (ATNF) pulsar catalog (Manchester et al. 2005) contains data for 368 pulsars (out of a total of 2264) consistent with this criterion.¹⁵⁰ The majority of these ($\sim 90\%$) are recycled MSPs that have been spun-up to high rotation frequencies by accretion from a binary companion which may still be present (see, e.g., Lorimer 2008, for an overview of MSPs and binary pulsars). MSPs spin down slowly (with \dot{f}_{rot} between approximately -10^{-14} and -10^{-17} Hz s⁻¹)

¹⁴⁸ For this analysis, the results were produced with version 6.16 of the LSC Algorithm Library Suite (LALSuite) <https://www.lsc-group.phys.uwm.edu/daswg/projects/lalsuite.html>.

¹⁴⁹ The \mathcal{F}/\mathcal{G} -statistic is most suitable for signal detection, whilst the upper limit derived from it here is mainly given for completeness. In the future a more sophisticated method, such as that of Feldman & Cousins (1998), may be used to produce frequentist confidence intervals for this analysis.

¹⁵⁰ ATNF pulsar catalog v1.47 <http://www.atnf.csiro.au/people/pulsar/psrcat/>

Table 2
Electromagnetic Observation Epochs for the
High Interest Pulsars

| MJD and Date |
|---|
| J0534+2200 (Crab pulsar) |
| 54997 (2009 Jun 15) – 55814 (2011 Sep 10) |
| J0537–6910 (N157B) |
| 54897 (2009 Mar 7) – 55041 (2009 Jul 29) |
| 55045 (2009 Aug 2) – 55182 (2009 Dec 17) |
| 55185 (2009 Dec 20) – 55263 (2010 Mar 8) |
| 55275 (2010 Mar 20) – 55445 (2010 Sep 6) |
| 55458 (2010 Sep 19) – 55503 (2010 Nov 3) |
| J0835–4510 (Vela pulsar) |
| 54983 (2009 Jun 1) – 55286 (2010 Mar 31) |
| 55713 (2011 Jun 1) – 55827 (2011 Sep 23) |
| J1813–1246 |
| 54693 (2008 Aug 15) – 55094 (2009 Sep 20) |
| 55094 (2009 Sep 20) – 55828 (2011 Sep 24) |
| J1833–1034 (G21.5–0.9) |
| 55041 (2009 Jul 29) – 55572 (2011 Jan 11) |
| J1913+1011 |
| 54867 (2009 Feb 5) – 55899 (2011 Dec 4) |
| J1952+3252 (CTB 80) |
| 54589 (2008 May 3) – 55325 (2010 May 9) |
| 55331 (2010 May 15) – 55802 (2011 Aug 29) |

and have characteristic ages¹⁵¹ greater than a few times 10^8 yr, implying a comparatively weak surface polar magnetic field ($10^8 \text{ G} \lesssim B_s \lesssim 10^9 \text{ G}$, via the relation for an orthogonal rotator with radius 10 km and $I_{zz} = I_{38}$ of $B_s = 3.3 \times 10^{19} (|\dot{f}_{\text{rot}}|/f_{\text{rot}}^3)^{1/2} \text{ G}$) compared to “normal” pulsars. About 10% are young pulsars with \dot{f}_{rot} between approximately -10^{-10} and $-10^{-12} \text{ Hz s}^{-1}$, characteristic ages of between ~ 1000 and a few tens of thousands of years, and therefore with the large implied surface magnetic fields of “normal” pulsars, $B_s \sim 10^{12} \text{ G}$. They are situated towards the low-frequency end of our sensitivity range.

Young pulsars have large spin-downs and relatively low frequencies, so in general have the highest gravitational wave spin-down limits, see Equation (5). This makes them particularly important targets as the limits can be within reach of current detectors. Equations (3) and (6) show that to produce emission at around the spin-down limit the required mass quadrupole/ellipticity would have to be large, at a level consistent with only the most exotic neutron star equations of state (see the discussion in Section 4). Such strong emission is unlikely, but its detection would have profound implications. Young pulsars also often show rotational anomalies such as glitches and timing noise (see, e.g., Helfand et al. 1980). The underlying causes of such phenomena are still quite uncertain, and gravitational wave data would be a powerful constraint. For the MSPs, the spin-down limits are generally several orders of magnitude below those for the young pulsars. They are located, however, in a more sensitive frequency range.

¹⁵¹ Characteristic age is given by $\tau = -(1/(n-1))(f_{\text{rot}}/\dot{f}_{\text{rot}})$, which, for a magnetic dipole braking index of $n = 3$, gives $\tau = -f_{\text{rot}}/(2\dot{f}_{\text{rot}})$, and for purely gravitational wave (quadrupole) spin-down would be $n = 5$, giving $\tau = -f_{\text{rot}}/(4\dot{f}_{\text{rot}})$ (a “gravitar,” Palomba 2005; Knispel & Allen 2008).

2.1. Electromagnetic Pulsar Observations

For this analysis, we have obtained ephemerides using radio, X-ray and γ -ray observations. The radio telescope observations have come from a variety of sources: the 12.5-m telescope and Lovell telescope at Jodrell Bank in the UK, the 26-m telescope at Hartebeesthoek in South Africa, the 15-m eXperimental Development Model (XDM) telescope in South Africa, the Giant Metrewave Radio Telescope (GMRT) in India, the Robert C. Byrd Green Bank Radio Telescope in the US, the Parkes radio telescope in Australia, the Nançay Decimetric Radio Telescope in France and the Hobart radio telescope in Australia. High energy X-ray and γ -ray timings have been obtained from the *Rossi X-ray Timing Explorer (RXTE)* and the *Fermi Large Area Telescope (LAT)*.

In total, for this analysis, we collected timing solutions for 179 pulsars. This selection includes 73 pulsars that have not been previously studied. However, for five of the pulsars targeted in the S3/S4 analysis (Abbott et al. 2007a) and another eleven of the pulsars targeted in the S5 analysis (Abbott et al. 2010), new coherent timing solutions were not available, so these stars¹⁵² have not been included in this search.

2.1.1. High Interest Targets

As discussed in Abbott et al. (2008),¹⁵³ due to our ignorance of the correct neutron star equation of state there is a large uncertainty in the moments of inertia for our targets, from 1 to $3 \times 10^{38} \text{ kg m}^2$. Therefore, the canonical spin-down limit estimates could be increased by a factor of ~ 1.7 . Also, there are uncertainties in some pulsar distance measurements of up to a factor of two which could further increase or decrease the spin-down limit. We therefore identified all sources that were within a factor of four of the canonical spin-down limit as worthy of special attention. Seven of the pulsars for which we have obtained timing solutions beat, or approach to within a factor of four, this limit. The electromagnetic observation epochs for each pulsar (which include each inter-glitch epoch for pulsars that glitched during the analysis) are given in Table 2.

Further details of these observations are given below:

J0534+2200 (the Crab pulsar). We have used the Jodrell Bank Monthly Ephemeris (Lyne et al. 1993) to track the phase of the Crab pulsar over the period of our runs. This ephemeris has timing solutions using the DE200 solar system ephemeris and the Barycentric Dynamical Time (TDB) time coordinate system. During S6/VSR2,4 the pulsar did not show signs of any timing glitches.

J0537–6910 (N157B). Long-term X-ray timing has been performed with the *RXTE* (Middleitch et al. 2006). Recent data covering S6 shows four glitches over the span of our science runs and the ephemerides for each inter-glitch epoch are given in the Appendix. The timing solutions used the DE200 solar system ephemeris (see Marshall et al. 1998) and the TDB time coordinate system. Several more glitches have been observed since the end of our science runs, but we do not report on them here.

¹⁵² The five additional pulsars targeted in S3/S4 were J1435–6100, J1629–6902, J1757–5322, J1911+0101A and J1911+0101B and the eleven additional pulsars targeted in S5 were J1701–3006B, J1701–3006C, J1748–2446P, J1748–2446ad, J1824–2452B, J1824–2452C, J1824–2452E, J1824–2452F, J1824–2452G, J1824–2452H, J1824–2452J.

¹⁵³ Note that Johnson-McDaniel (2013) computes even larger potential moments of inertia at $\sim 5 \times 10^{38} \text{ kg m}^2$ for some solid quark stars.

J0835–4510 (the Vela pulsar). Radio observations over the period of VSR2 were taken with the Hobart radio telescope in Tasmania and the Hartebeesthoek 26-m radio telescope in South Africa (Abadie et al. 2011). Radio timing over the VSR4 run was performed with the XDM telescope and the 26-m telescope at Hartebeesthoek. The timing solutions have used the DE405 solar system ephemeris and the Barycentric Coordinate Time (TCB) time coordinate system. Vela was observed to glitch on 2010 July 31 (Buchner 2010), between VSR2 and VSR4, but it has not glitched since then.

J1813–1246. This pulsar was discovered in a search of gamma-ray data from the *Fermi* LAT (Abdo et al. 2009), and using the unbinned maximum likelihood methods of Ray et al. (2011) timing measurements were made covering all our runs. It was observed to glitch once during this time on 2009 September 20. Pre-and-post glitch timing solutions have been produced using the DE405 solar system ephemeris and the TDB time coordinate system.

J1833–1034 (G21.5–0.9). The period from the start of S6/VSR2 until 2011 January is covered by observations made with the GMRT (Roy et al. 2012). During this period, one glitch was observed, with a best fit epoch of 2009 November 6 (MJD 55142±2). To remove its effect, an ephemeris fit was performed on timing data excluding 80 days after the glitch. The timing solution uses the DE405 solar system ephemeris and the TDB time coordinate system.

J1913+1011. This pulsar was observed at Jodrell Bank and showed no timing anomalies over the science runs. The timing solution uses the DE405 solar system ephemeris and the TDB time coordinate system.

J1952+3252 (CTB 80). This pulsar was observed over the whole of our science runs at Nançay and Jodrell Bank. It glitched on 2010 May 11 (MJD 55327), between the end of S6/VSR2 and the start of VSR4. Phase incoherent pre- and post-glitch timing solutions have been produced using the DE405 solar system ephemeris and the TCB time ephemeris. The solution include fits to the timing noise using the TEMPO2 FITWAVES method described in Hobbs et al. (2006).

For several of these pulsars potential constraints on their orientations (the inclination ι and polarization angle ψ ¹⁵⁴) are available from observations of their pulsar wind nebulae (Ng & Romani 2004, 2008). These are listed in Table 3 where the uncertainties used are estimated from the systematic and statistical values given in Ng & Romani (2004, 2008), and the mean angle value is used if multiple fits are given (e.g., fits to the inner and outer tori of the Crab pulsar wind nebula). We briefly discussed how these constraints are used in the analyses in Section 1.3.

For J0534+2200 and J0537–6910, the Bayesian method also makes use of results from the LIGO S5 run (Abbott et al. 2010) as a prior on the h_0 and $\cos \iota$ parameters. During S5, both of these pulsars glitched, and the data for each inter-glitch period was analyzed independently. Results were also produced assuming that the data could be analyzed coherently over the glitches.

¹⁵⁴ In Ng & Romani (2008) the inclination is denoted by ζ and the position angle Ψ is equivalent to our polarization angle. Our searches are insensitive to rotations of 90° in the polarization angle, so our quoted values are rotated into the range $-45^\circ < \psi < 45^\circ$.

Table 3
Implied Orientations of Pulsars from their Pulsar Wind Nebulae Observations
(Ng & Romani 2004, 2008)

| Pulsar | ι | ψ |
|--------------------------|----------------------------|-----------------------------|
| J0534+2200 (Crab pulsar) | $62^\circ 2 \pm 1^\circ 9$ | $35^\circ 2 \pm 1^\circ 5$ |
| J0537–6910 | $92^\circ 8 \pm 0^\circ 9$ | $41^\circ 0 \pm 2^\circ 2$ |
| J0835–4510 (Vela pulsar) | $63^\circ 6 \pm 0^\circ 6$ | $40^\circ 6 \pm 0^\circ 1$ |
| J1833–1034 | $85^\circ 4 \pm 0^\circ 3$ | $45^\circ \pm 1^\circ$ |
| J1952+3252 ^a | ... | $-11^\circ 5 \pm 8^\circ 6$ |

Note. ^a The polarization angle is not taken from a fit to the pulsar wind nebula, but instead is the average of the angle calculated from proper motion measurements and H α observations of a bow shock (Ng & Romani 2004).

To avoid the assumptions about coherence over the glitches, we have used the independent inter-glitch results that gave the lowest h_0 as the prior for the current analysis (see Table 3 of Abbott et al. 2010).

3. RESULTS

None of the searches yielded evidence of a gravitational wave signal, and upper limits have been placed on signal strengths. These limits are subject to the uncertainties in the amplitude calibration, as discussed in Section 1.2. For the joint results, which combine data from multiple detectors, the sensitivity is often dominated by the most sensitive instrument. Therefore, we expect the amplitude uncertainty due to calibration uncertainties to also be dominated by the most sensitive instrument. So, following the calibration error given in Section 1.2, below ~ 50 Hz we have an amplitude uncertainty of $\sim 6\%$, and above that we have uncertainty of $\sim 20\%$. The phase uncertainties are small enough to have a negligible contribution to the possible amplitude uncertainty.

3.1. Data Selection

As discussed in Section 2.1, for a few pulsars the electromagnetic observations did not always span the S6/VSR2,4 runs completely, and some pulsars glitched during the runs. As a result, we deal with these instances separately. In most cases, we can use all the data coherently, but, in other cases, sections of data must be combined incoherently. The relative sensitivities of the detectors at the pulsar frequencies also dictate whether we have used Virgo-only, LIGO-only or Virgo and LIGO data (see Figure 1). For J0537–6910, only the LIGO data has been used because of its better sensitivity at the corresponding frequency, and results from each inter-glitch period have been combined incoherently. For J0835–4510 (the Vela pulsar), a glitch occurred just prior to VSR4 and we had no phase-connected timing solution between VSR2 (Abadie et al. 2011) and VSR4 epochs. The VSR2 results and VSR4 data have therefore been incoherently combined. For J1813–1246, the results from the pre- and post-glitch periods using all data from S6 and VSR2,4 have been combined incoherently. For J1833–1034, only VSR2 data up to the time of the observed glitch has been used.

The parameters and results (from the three different analyses discussed in Section 1.3) for the seven pulsars highlighted in Section 2.1 are given in Tables 4 and 5, respectively. Table 5 gives the 95% upper limit on the gravitational wave amplitude, $h_0^{95\%}$, the equivalent limits (via Equation (3)) on the stars fiducial ellipticity, ε , and mass quadrupole moment, Q_{22} , the ratio of the limit to the spin-down limit, $h_0^{95\%}/h_0^{\text{sd}}$, and the limit on the gravitational wave luminosity compared to the total spin-down luminosity. This final value is given in the form of the percentage

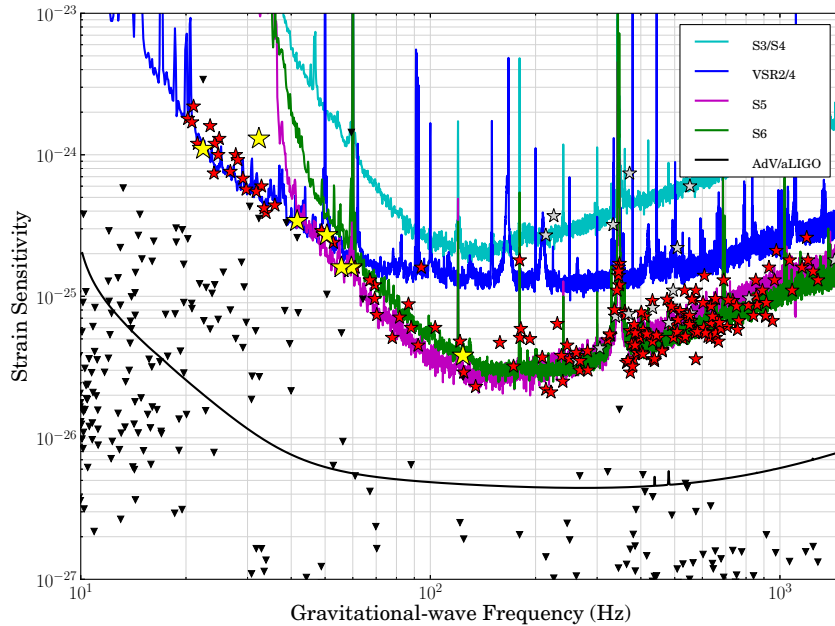


Figure 1. $h_0^{95\%}$ upper limits (given by ★) for 195 pulsars from the LIGO and Virgo S3/S4, S5, S6, VSR2, and VSR4 runs. The curves give estimated relative strain sensitivities of these runs and potential future science runs. The sensitivities are based on the harmonic mean of the observation time (T) weighted one-sided power spectral densities S_n from all detectors operating during the given run, and are given by $10.8\sqrt{S_n/T}$, where the scale factor of 10.8 is given in Dupuis & Woan (2005). The AdV/aLIGO curve assumes a joint analysis of two equally sensitive advanced LIGO detectors and the advanced Virgo detector operating at their full design sensitivities with one year of coherent integration (the sensitivity curves are those given in Aasi et al. 2013c). The ▼ give the spin-down limits for all (non-Globular Cluster) pulsars, based on values taken from the ATNF catalog and assuming the canonical moment of inertia. The ★ show the observational upper limits from Tables 5, 6, and 7, with the seven high interest pulsars represented by the larger, lighter colored stars. Results for pulsars using the previous S3/S4 and S5 data are given by the small lighter colored stars.

(A color version of this figure is available in the online journal.)

Table 4
The Properties of the Pulsars of High Interest

| Pulsar | α | δ | f_{rot} (Hz) | f_{gw} (Hz) | \dot{f}_{rot} (Hz s $^{-1}$) | d (kpc) | \dot{E}^a (W) | $h^{\text{sd}a}$ |
|------------------------|---|---------------|--------------------------|-------------------------|---|-------------------|----------------------|-----------------------|
| J0534+2200 (Crab) | 05 ^h 34 ^m 31 ^s .97 | 22°00′52″.07 | 29.72 | 59.44 | -3.7×10^{-10} | 2.0 ^b | 4.6×10^{31} | 1.4×10^{-24} |
| J0537–6910 (N157B) | 05 ^h 37 ^m 47 ^s .36 | –69°10′20″.40 | 61.97 | 123.94 | -2.0×10^{-10} | 50.0 ^c | 4.9×10^{31} | 3.0×10^{-26} |
| J0835–4510 (Vela) | 08 ^h 35 ^m 20 ^s .61 | –45°10′34″.88 | 11.19 | 22.39 | -1.6×10^{-11} | 0.29 ^d | 6.9×10^{29} | 3.3×10^{-24} |
| J1813–1246 | 18 ^h 13 ^m 23 ^s .74 | –12°46′00″.86 | 20.80 | 41.60 | -7.6×10^{-12} | 1.9 ^e | 6.2×10^{29} | 2.6×10^{-25} |
| J1833–1034 (G21.5–0.9) | 18 ^h 33 ^m 33 ^s .61 | –10°34′16″.61 | 16.16 | 32.33 | -5.3×10^{-11} | 4.8 ^f | 3.4×10^{30} | 3.0×10^{-25} |
| J1913+1011 | 19 ^h 13 ^m 20 ^s .34 | 10°11′23″.11 | 27.85 | 55.70 | -2.6×10^{-12} | 4.5 ^g | 2.8×10^{29} | 2.3×10^{-25} |
| J1952+3252 (CTB 80) | 19 ^h 52 ^m 58 ^s .11 | 32°52′41″.24 | 25.30 | 50.59 | -3.7×10^{-12} | 3.0 ^g | 3.7×10^{29} | 1.0×10^{-25} |

Notes.

^a The spin-down luminosity, \dot{E} , and spin-down gravitational wave amplitude limit, h^{sd} , both assume a canonical moment of inertia of $I_{zz} = 10^{38}$ kg m 2 .

^b See Appendix of Kaplan et al. (2008).

^c Pietrzyński et al. (2013).

^d Dodson et al. (2003).

^e This distance is the average of the two estimates from Wang (2011), which allow a distance between ~ 0.9 –3.5 kpc.

^f Tian & Leahy (2008).

^g The distance is taken from the ATNF pulsar catalog (Manchester et al. 2005).

of the spin-down luminosity required to produce a gravitational wave at the amplitude limit (it can be seen from Equation (4) that this is just the square of the ratio $h_0^{95\%}/h_0^{\text{sd}}$). For those pulsars with constrained orientations (see Table 3) the results with and without the constraints are also given in Table 5. Despite the very tight constraints given in Table 3 it should be noted that these results would only show minor differences if the angle (ι and ψ) errors were expanded to several times the given values. This is because the recovered posterior probability distributions on these parameters are slowly and smoothly varying over their parameter ranges. A brief discussion of the differences between the upper limits from the different methods is given in Section 1.3.

One of the new targets, J1824–2452I (which is an interesting pulsar that is seen to switch between being accretion and rotation powered; Papitto et al. 2013), had a coherent timing solution that covered 2006, so S5 data from the LIGO detectors has been reanalyzed for this result. For all other pulsars, we have used only the VSR2 and VSR4 data if $f_{\text{gw}} < 40$ Hz, and have coherently combined VSR2, VSR4 and S6 data from H1 and L1 for pulsars with $f_{\text{gw}} > 40$ Hz. All the available science mode data (i.e., when the detectors were operating in a stable state) has been used, with details given in Table 1.

For the 19 pulsars with $f_{\text{gw}} < 40$ Hz the results can be found in Table 6. Because of their low frequencies, none of these pulsars had been targeted before.

Table 5
Upper Limits for the High Interest Pulsars^a

| Analysis | $h_0^{95\%}$ | ε | Q_{22} (kg m ²) | $h_0^{95\%}/h_0^{\text{sd}}$ | $\dot{E}_{\text{gw}}/\dot{E}$ % |
|--------------------------------------|----------------------------|----------------------------|-------------------------------|------------------------------|---------------------------------|
| J0534+2200 (Crab) | | | | | |
| Bayesian | $1.6(1.4) \times 10^{-25}$ | $8.6(7.5) \times 10^{-5}$ | $6.6(5.8) \times 10^{33}$ | 0.11 (0.10) | 1.2 (1.0) |
| \mathcal{F}/\mathcal{G} -statistic | $2.3(1.8) \times 10^{-25}$ | $12.3(9.6) \times 10^{-5}$ | $11.6(7.4) \times 10^{33}$ | 0.16 (0.13) | 2.6 (1.7) |
| 5 <i>n</i> -vector | $1.8(1.6) \times 10^{-25}$ | $9.7(8.6) \times 10^{-5}$ | $7.4(6.6) \times 10^{33}$ | 0.12 (0.11) | 1.4 (1.2) |
| J0537–6910 | | | | | |
| Bayesian | $3.8(4.4) \times 10^{-26}$ | $1.2(1.4) \times 10^{-4}$ | $0.9(1.0) \times 10^{34}$ | 1.4 (1.7) | 200 (290) |
| \mathcal{F}/\mathcal{G} -statistic | $1.1(1.0) \times 10^{-25}$ | $3.4(3.1) \times 10^{-4}$ | $2.6(2.4) \times 10^{34}$ | 4.1 (3.9) | 1700 (1500) |
| 5 <i>n</i> -vector | $4.5(6.7) \times 10^{-26}$ | $1.4(2.1) \times 10^{-4}$ | $1.1(1.6) \times 10^{34}$ | 1.6 (2.4) | 260 (580) |
| J0835–4510 (Vela) | | | | | |
| Bayesian | $1.1(1.0) \times 10^{-24}$ | $6.0(5.5) \times 10^{-4}$ | $4.7(4.2) \times 10^{34}$ | 0.33 (0.30) | 11 (9.0) |
| \mathcal{F}/\mathcal{G} -statistic | $4.2(9.0) \times 10^{-25}$ | $2.3(4.9) \times 10^{-4}$ | $1.8(3.8) \times 10^{34}$ | 0.13 (0.27) | 1.7 (7.3) |
| 5 <i>n</i> -vector | $1.1(1.1) \times 10^{-24}$ | $6.0(6.0) \times 10^{-4}$ | $4.7(4.7) \times 10^{34}$ | 0.33 (0.33) | 11 (11) |
| J1813–1246 | | | | | |
| Bayesian | 3.4×10^{-25} | 3.5×10^{-4} | 2.7×10^{34} | 1.3 | 170 |
| \mathcal{F}/\mathcal{G} -statistic | 7.1×10^{-25} | 7.4×10^{-4} | 5.7×10^{34} | 2.7 | 730 |
| 5 <i>n</i> -vector | 4.8×10^{-25} | 4.9×10^{-4} | 3.8×10^{34} | 1.8 | 320 |
| J1833–1034 | | | | | |
| Bayesian | $1.3(1.4) \times 10^{-24}$ | $5.7(6.1) \times 10^{-3}$ | $4.4(4.7) \times 10^{35}$ | 4.3 (4.6) | 1800 (2100) |
| \mathcal{F}/\mathcal{G} -statistic | $1.2(1.2) \times 10^{-24}$ | $5.2(5.2) \times 10^{-3}$ | $4.0(4.0) \times 10^{35}$ | 3.9 (3.9) | 1500 (1500) |
| 5 <i>n</i> -vector | $1.4(2.0) \times 10^{-24}$ | $6.1(8.7) \times 10^{-3}$ | $4.7(6.7) \times 10^{35}$ | 4.6 (6.6) | 2100 (4400) |
| J1913+1011 | | | | | |
| Bayesian | 1.6×10^{-25} | 2.2×10^{-4} | 1.7×10^{34} | 2.9 | 840 |
| \mathcal{F}/\mathcal{G} -statistic | 2.9×10^{-25} | 4.1×10^{-4} | 3.1×10^{34} | 5.3 | 2800 |
| 5 <i>n</i> -vector | 2.5×10^{-25} | 3.4×10^{-4} | 2.7×10^{34} | 4.5 | 2000 |
| J1952+3252 | | | | | |
| Bayesian | $2.7(2.5) \times 10^{-25}$ | $3.0(2.8) \times 10^{-4}$ | $2.3(2.1) \times 10^{34}$ | 2.6 (2.5) | 680 (630) |
| \mathcal{F}/\mathcal{G} -statistic | 6.0×10^{-25} | 6.7×10^{-4} | 5.1×10^{34} | 5.8 | 3400 |
| 5 <i>n</i> -vector | $3.1(3.2) \times 10^{-25}$ | $3.4(3.5) \times 10^{-4}$ | $2.6(2.7) \times 10^{34}$ | 3.0 (3.1) | 900 (960) |

Notes. Limits with constrained orientations are given in parentheses.

^a Detector calibration errors mean that for pulsars with f_{gw} below and above 50 Hz (see Table 4) there are $\sim 6\%$ and $\sim 20\%$ uncertainties respectively on these limits.

Results for pulsars with $f_{\text{gw}} > 40$ Hz using S6 and VSR2,4 are shown in Table 7. Distances to pulsars in Terzan 5 (with designations J1748–2446) are assumed to be 5.5 kpc (Ortolani et al. 2007) rather than the value of 8.7 kpc given in the ATNF catalog, and distances to the pulsars in M28 (with designations J1824–2452) are assumed to be 5.5 kpc (Harris 1996) rather than the distance of 4.9 kpc given in Abbott et al. (2010). Unless otherwise specified in the table for all other pulsars we use the distance values given by the DIST value in the ATNF catalog (Manchester et al. 2005), which generally are dispersion measure calculations from the electron density distribution model of Taylor & Cordes (1993). For the 16 pulsars where new timing solutions were not available during the most recent runs (see Section 2.1), we include the results from the LIGO S3/S4 (Abbott et al. 2007a) and S5 analysis (Abbott et al. 2010).

The gravitational wave amplitude upper limits as a function of frequency are plotted in Figures 1 and 2 (showing a version just containing the seven high interest pulsars), which also show bands giving the expected sensitivity of the analysis. The upper limits in histogram form for all pulsars can be seen in Figure 3. The histograms show that the distribution of h_0 upper limits is peaked just below 10^{-25} , corresponding to equivalent peaks on ε and Q_{22} of $\sim 10^{-6}$ and $\sim 10^{-32}$ kg m². The spin-down limit ratios shows that we are within a factor of 100 for just over half

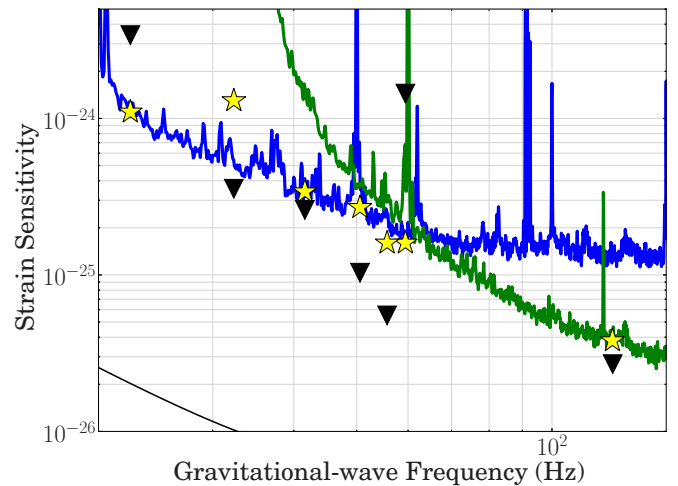


Figure 2. Zoomed version of Figure 1 focusing on the seven high interest pulsars. The outlier at ~ 32 Hz is J1833–1034 for which only VSR2 data was used.

(A color version of this figure is available in the online journal.)

of the pulsars. It is interesting to see that due to the shape of the detector sensitivity curves the lower frequency young pulsars (analyzed only with Virgo data) have the highest amplitude limits, but as several have high spin-down luminosities they

Table 6
Limits on the Gravitational Wave Amplitude for Known Pulsars with $f_{\text{gw}} < 40$ Hz Using VSR2,4 Data

| Pulsar | f_{rot} (Hz) | f_{gw} (Hz) | \dot{f}_{rot} (Hz s ⁻¹) | d (kpc) | h_0^{sd} | $h_0^{95\%}$ | ε | Q_{22} (kg m ²) | $h_0^{95\%}/h_0^{\text{sd}}$ |
|-------------|--------------------------|-------------------------|---|--------------|-------------------------------|------------------------|----------------------|----------------------------------|------------------------------|
| J0106+4855 | 12.03 | 24.05 | -6.2×10^{-14} | 7.3 | 7.9×10^{-27} | 7.4×10^{-25} | 8.9×10^{-3} | 6.9×10^{35} | 94 |
| J0609+2130 | 17.95 | 35.91 | -7.6×10^{-17} | 1.8 | 9.1×10^{-28} | 4.4×10^{-25} | 5.9×10^{-4} | 4.6×10^{34} | 490 |
| J1528-3146 | 16.44 | 32.88 | -6.7×10^{-17} | 1.0 | 1.6×10^{-27} | 6.0×10^{-25} | 5.2×10^{-4} | 4.0×10^{34} | 360 |
| J1718-3825 | 13.39 | 26.78 | -2.4×10^{-12} | 4.2 | 8.0×10^{-26} | 7.6×10^{-25} | 4.2×10^{-3} | 3.3×10^{35} | 9.5 |
| J1747-2958 | 10.12 | 20.24 | -6.3×10^{-12} | 2.5 | 2.6×10^{-25} | 1.8×10^{-24} | 1.0×10^{-2} | 7.9×10^{35} | 7.0 |
| J1748-2446J | 12.45 | 24.89 | -2.0×10^{-16} | 5.5 | $5.8 \times 10^{-28\text{a}}$ | 1.3×10^{-24} | 1.1×10^{-2} | 8.3×10^{35} | 2200 |
| J1753-1914 | 15.88 | 31.77 | -4.9×10^{-16} | 2.8 | 1.6×10^{-27} | 5.5×10^{-25} | 1.4×10^{-3} | 1.1×10^{35} | 340 |
| J1753-2240 | 10.51 | 21.02 | -6.9×10^{-17} | 3.5 | 6.0×10^{-28} | 2.2×10^{-24} | 1.6×10^{-2} | 1.3×10^{36} | 3700 |
| J1809-1917 | 12.08 | 24.17 | -3.7×10^{-12} | 3.7 | 1.2×10^{-25} | 1.2×10^{-24} | 7.2×10^{-3} | 5.6×10^{35} | 9.9 |
| J1828-1101 | 13.88 | 27.76 | -2.9×10^{-12} | 7.3 | 5.0×10^{-26} | 1.0×10^{-24} | 9.2×10^{-3} | 7.1×10^{35} | 20 |
| J1831-0952 | 14.87 | 29.73 | -1.8×10^{-12} | 4.3 | 6.5×10^{-26} | 5.7×10^{-25} | 2.6×10^{-3} | 2.0×10^{35} | 8.7 |
| J1833-0827 | 11.72 | 23.45 | -1.3×10^{-12} | 4.5 | $5.9 \times 10^{-26\text{b}}$ | 1.6×10^{-24} | 1.2×10^{-2} | 9.6×10^{35} | 27 |
| J1856+0245 | 12.36 | 24.72 | -9.5×10^{-12} | 10.3 | 6.9×10^{-26} | 10.0×10^{-25} | 1.6×10^{-2} | 1.2×10^{36} | 15 |
| J1904+0412 | 14.07 | 28.13 | -2.8×10^{-17} | 4.0 | 2.8×10^{-28} | 9.2×10^{-25} | 4.4×10^{-3} | 3.4×10^{35} | 3300 |
| J1915+1606 | 16.94 | 33.88 | -2.5×10^{-15} | 7.1 | $1.4 \times 10^{-27\text{b}}$ | 3.9×10^{-25} | 2.3×10^{-3} | 1.7×10^{35} | 280 |
| J1928+1746 | 14.55 | 29.10 | -2.8×10^{-12} | 8.1 | 4.3×10^{-26} | 6.8×10^{-25} | 6.2×10^{-3} | 4.8×10^{35} | 16 |
| J1954+2836 | 10.79 | 21.57 | -2.5×10^{-12} | 1.6 | 2.4×10^{-25} | 1.2×10^{-24} | 4.0×10^{-3} | 3.1×10^{35} | 5.1 |
| J2043+2740 | 10.40 | 20.80 | -1.3×10^{-13} | 1.1 | 8.1×10^{-26} | 1.7×10^{-24} | 4.1×10^{-3} | 3.2×10^{35} | 21 |
| J2235+1506 | 16.73 | 33.46 | -2.9×10^{-17} | 1.1 | $9.2 \times 10^{-28\text{b}}$ | 4.2×10^{-25} | 4.0×10^{-4} | 3.1×10^{34} | 450 |

Notes. Detector calibration errors mean that for these pulsars there are $\sim 6\%$ uncertainties on these limits.

^a The pulsar's spin-down is calculated using a characteristic spin-down age of 10^9 yr.

^b The pulsar's spin-down is corrected for proper motion effects.

have an approximately uniform spread in spin-down limit ratios.

4. DISCUSSION

We have seen no credible evidence for gravitational wave emission from any known pulsar, but have been able to place upper limits on the gravitational wave amplitude from an unprecedented number of pulsars. In this work we have produced entirely new results for 73 pulsars and updated the results of previously searches for 106 pulsars, with results from a further 16 from previous analyses being reproduced here. A total of 195 pulsars have now been targeted over the lifetimes of the first generation of interferometric gravitational wave detectors.

4.1. Quadrupole Estimates

As discussed in the introduction, we have targeted the gravitational-wave signature of the time-varying $l = m = 2$ quadrupole moment. There is great uncertainty, however, as to whether neutron stars can form and sustain sufficient elastic deformations to give an observable quadrupole, and this, in turn, makes it difficult to model a realistic source population. The recent work by Johnson-McDaniel & Owen (2013) (also see, e.g., Owen 2005; Pitkin 2011) on the maximum sustainable quadrupole for a variety of neutron star equations of state indicates that relatively large quadrupoles can indeed be sustained. Johnson-McDaniel & Owen (2013) find that solid quark stars could sustain quadrupoles of up to 10^{37} kg m² (or fiducial ellipticities of order 0.1), hybrid stars could sustain quadrupoles of up to 10^{35} kg m² (or fiducial ellipticities of order 1×10^{-3}), while for normal neutron stars the stiffest equations of state allow quadrupoles of $\sim 1 \times 10^{33}$ kg m² (or fiducial ellipticities of $\sim 1 \times 10^{-5}$). It is worth noting that these are maximum allowable quadrupoles, and it is still unknown whether they are realized in nature for reasons described in Abbott et al. (2007b).

A mass quadrupole may also be generated by distortional pressure from the star's magnetic field (see, e.g., Bonazzola &ourgoulhon 1996; Cutler 2002; Ciolfi et al. 2010). The external dipole field of a pulsar is usually estimated from its rotational spin-down, assuming this is due to magnetic dipole radiation (equivalent to the gravitational wave spin-down limit that we define). As discussed in Section 2, this gives external surface dipole field strengths of $\sim 10^9$ G for MSPs and $\sim 10^{12}$ G for normal pulsars. Internal fields of this magnitude are too small to induce mass quadrupoles that would be currently observable, but the field strengths of some magnetars are at a suitable level (though rotating too slowly to be detectable sources for ground-based gravitational wave detectors). Unfortunately, internal field strengths and configurations are not well understood, and the mechanisms for burying fields beneath the surface are uncertain. Studies of one young pulsar with a braking index of $n \approx 1$ (Espinoza et al. 2011) may point towards an evolving and increasing external magnetic field, with an internal field leaking out over time, but recently other mechanisms have been proposed to explain the evolution of the field that do not rely on an increasing magnetic field (e.g., Ho & Andersson 2012; Çalişkan et al. 2013). Mastrano & Melatos (2012) discuss the prospects of constraining field strength and configuration for recycled MSPs using gravitational wave data. This is also discussed in Pitkin (2011), who shows limits that could be obtained on fully poloidal or toroidal field configurations. Further estimates of the quadrupoles that can be generated by internal magnetic fields for a given equation of state are given in Haskell et al. (2008, 2009), Akgun & Wasserman (2007).

4.2. High Interest Pulsars

For the seven high interest pulsars the results are all close to (or beat) the spin-down limits. In particular, our upper limits are significantly below the spin-down limit for the Crab and Vela pulsars, further improving over past results. The mass

Table 7
Limits on the Gravitational Wave Amplitude for Known Pulsars with $f_{\text{gw}} > 40$ Hz

| Pulsar | f_{rot} (Hz) | f_{gw} (Hz) | \dot{f}_{rot} (Hz s ⁻¹) | d (kpc) | h_0^{sd} | Prior $h_0^{95\%}$ | S6/VSR2.4 $h_0^{95\%}$ | ε | Q_{22} (kg m ²) | $h_0^{95\%}/h_0^{\text{sd}}$ |
|--------------------------|--------------------------|-------------------------|---|------------------|------------------------|-----------------------|------------------------|----------------------|----------------------------------|------------------------------|
| J0023+0923 | 327.85 | 655.69 | -1.3×10^{-15} | 0.9 | 1.7×10^{-27} | ... | 6.9×10^{-26} | 1.5×10^{-7} | 1.1×10^{31} | 41 |
| J0024-7204C | 173.71 | 347.42 | 1.6×10^{-15} | 4.0 | 6.1×10^{-28a} | 5.8×10^{-25} | 1.7×10^{-25} | 5.5×10^{-6} | 4.2×10^{32} | 290 |
| J0024-7204D | 186.65 | 373.30 | 1.6×10^{-16} | 4.0 | 1.8×10^{-28a} | 4.5×10^{-26} | 2.9×10^{-26} | 7.8×10^{-7} | 6.1×10^{31} | 160 |
| J0024-7204E | 282.78 | 565.56 | -7.8×10^{-15} | 4.0 | 1.1×10^{-27a} | 9.9×10^{-26} | 9.7×10^{-26} | 1.1×10^{-6} | 8.9×10^{31} | 92 |
| J0024-7204F | 381.16 | 762.32 | -9.3×10^{-15} | 4.0 | 9.9×10^{-28a} | 8.8×10^{-26} | 6.7×10^{-26} | 4.4×10^{-7} | 3.4×10^{31} | 67 |
| J0024-7204G | 247.50 | 495.00 | 2.6×10^{-15} | 4.0 | 6.6×10^{-28a} | 9.9×10^{-26} | 8.2×10^{-26} | 1.3×10^{-6} | 9.8×10^{31} | 120 |
| J0024-7204H | 311.49 | 622.99 | 3.0×10^{-16} | 4.0 | 2.0×10^{-28a} | 6.5×10^{-26} | 5.2×10^{-26} | 5.1×10^{-7} | 3.9×10^{31} | 260 |
| J0024-7204I | 286.94 | 573.89 | 3.9×10^{-15} | 4.0 | 7.4×10^{-28a} | 5.2×10^{-26} | 5.8×10^{-26} | 6.7×10^{-7} | 5.2×10^{31} | 79 |
| J0024-7204J | 476.05 | 952.09 | 2.4×10^{-15} | 4.0 | 4.5×10^{-28a} | 1.0×10^{-25} | 6.6×10^{-26} | 2.8×10^{-7} | 2.1×10^{31} | 150 |
| J0024-7204L | 230.09 | 460.18 | -3.6×10^{-15} | 4.0 | 8.0×10^{-28b} | 5.8×10^{-26} | 4.2×10^{-26} | 7.4×10^{-7} | 5.7×10^{31} | 52 |
| J0024-7204M | 271.99 | 543.97 | -4.3×10^{-15} | 4.0 | 8.0×10^{-28b} | 6.2×10^{-26} | 7.0×10^{-26} | 9.0×10^{-7} | 7.0×10^{31} | 88 |
| J0024-7204N | 327.44 | 654.89 | 2.5×10^{-15} | 4.0 | 5.6×10^{-28a} | 8.4×10^{-26} | 5.1×10^{-26} | 4.5×10^{-7} | 3.5×10^{31} | 91 |
| J0024-7204O | 378.31 | 756.62 | -4.2×10^{-15} | 4.0 | 6.7×10^{-28a} | 9.3×10^{-26} | 5.8×10^{-26} | 3.8×10^{-7} | 3.0×10^{31} | 86 |
| J0024-7204Q | 247.94 | 495.89 | -3.9×10^{-15} | 4.0 | 8.0×10^{-28b} | 5.8×10^{-26} | 5.1×10^{-26} | 7.9×10^{-7} | 6.1×10^{31} | 64 |
| J0024-7204R | 287.32 | 574.64 | -4.6×10^{-15} | 4.0 | 8.0×10^{-28b} | 5.6×10^{-26} | 3.6×10^{-26} | 4.1×10^{-7} | 3.2×10^{31} | 45 |
| J0024-7204S | 353.31 | 706.61 | -5.6×10^{-15} | 4.0 | 8.0×10^{-28b} | 6.9×10^{-26} | 6.1×10^{-26} | 4.6×10^{-7} | 3.6×10^{31} | 76 |
| J0024-7204T | 131.78 | 263.56 | -2.1×10^{-15} | 4.0 | 8.0×10^{-28b} | 3.3×10^{-26} | 3.8×10^{-26} | 2.0×10^{-6} | 1.6×10^{32} | 47 |
| J0024-7204U | 230.26 | 460.53 | -4.9×10^{-15} | 4.0 | 9.3×10^{-28a} | 5.7×10^{-26} | 4.1×10^{-26} | 7.2×10^{-7} | 5.6×10^{31} | 43 |
| J0024-7204Y | 455.24 | 910.47 | -7.2×10^{-15} | 4.0 | 8.0×10^{-28b} | 9.4×10^{-26} | 7.2×10^{-26} | 3.3×10^{-7} | 2.6×10^{31} | 90 |
| J0030+0451 | 205.53 | 411.06 | -4.3×10^{-16} | 0.3 | 4.1×10^{-27a} | ... | 7.2×10^{-26} | 1.1×10^{-7} | 8.7×10^{30} | 17 |
| J0034-0534 | 532.71 | 1065.43 | -1.5×10^{-16} | 1.0 | 4.4×10^{-28a} | ... | 1.8×10^{-25} | 1.5×10^{-7} | 1.1×10^{31} | 410 |
| J0218+4232 | 430.46 | 860.92 | -1.4×10^{-14} | 5.8 | 7.9×10^{-28a} | 1.5×10^{-25} | 8.7×10^{-26} | 6.5×10^{-7} | 5.0×10^{31} | 110 |
| J0307+7443 | 316.85 | 633.70 | -1.7×10^{-15} | 0.6 ^c | 3.3×10^{-27} | ... | 8.6×10^{-26} | 1.1×10^{-7} | 8.9×10^{30} | 26 |
| J0340+41 | 303.09 | 606.18 | -6.5×10^{-16} | 2.7 | 4.4×10^{-28} | ... | 5.6×10^{-26} | 3.8×10^{-7} | 3.0×10^{31} | 130 |
| J0407+1607 | 38.91 | 77.82 | -1.2×10^{-16} | 4.1 | 3.5×10^{-28} | 6.2×10^{-26} | 5.1×10^{-26} | 3.2×10^{-5} | 2.5×10^{33} | 140 |
| J0437-4715 | 173.69 | 347.38 | -4.1×10^{-16} | 0.2 | 7.8×10^{-27a} | 5.7×10^{-25} | 1.2×10^{-25} | 1.6×10^{-7} | 1.2×10^{31} | 16 |
| J0605+3757 ^d | 366.58 | 733.15 | -6.5×10^{-16} | 0.7 ^c | 1.6×10^{-27} | ... | 9.3×10^{-26} | 1.1×10^{-7} | 8.6×10^{30} | 59 |
| J0610-2100 | 258.98 | 517.96 | -2.3×10^{-16} | 5.6 | 1.3×10^{-28a} | ... | 7.9×10^{-26} | 1.6×10^{-6} | 1.2×10^{32} | 590 |
| J0613-0200 | 326.60 | 653.20 | -9.4×10^{-16} | 0.9 | 1.5×10^{-27a} | 1.1×10^{-25} | 5.6×10^{-26} | 1.1×10^{-7} | 8.6×10^{30} | 37 |
| J0614-3329 | 317.59 | 635.19 | -1.7×10^{-15} | 3.0 | 6.4×10^{-28} | ... | 8.5×10^{-26} | 5.9×10^{-7} | 4.5×10^{31} | 130 |
| J0621+1002 | 34.66 | 69.31 | -5.5×10^{-17} | 1.9 | 5.4×10^{-28a} | 1.5×10^{-25} | 9.6×10^{-26} | 3.6×10^{-5} | 2.7×10^{33} | 180 |
| J0711-6830 | 182.12 | 364.23 | -2.9×10^{-16} | 1.0 | 9.8×10^{-28a} | 5.0×10^{-26} | 3.4×10^{-26} | 2.5×10^{-7} | 2.0×10^{31} | 35 |
| J0737-3039A | 44.05 | 88.11 | -3.4×10^{-15} | 1.1 | 6.5×10^{-27a} | 7.8×10^{-26} | 6.0×10^{-26} | 8.0×10^{-6} | 6.2×10^{32} | 9.2 |
| J0751+1807 | 287.46 | 574.92 | -6.3×10^{-16} | 0.4 | 3.0×10^{-27a} | 1.6×10^{-25} | 1.1×10^{-25} | 1.2×10^{-7} | 9.6×10^{30} | 36 |
| J0900-3144 | 90.01 | 180.02 | -4.0×10^{-16} | 0.8 | 2.1×10^{-27} | ... | 1.8×10^{-25} | 4.3×10^{-6} | 3.3×10^{32} | 88 |
| J1012+5307 | 190.27 | 380.54 | -4.1×10^{-16} | 0.7 | 1.7×10^{-27a} | 6.9×10^{-26} | 4.6×10^{-26} | 2.1×10^{-7} | 1.6×10^{31} | 27 |
| J1017-7156 | 427.62 | 855.24 | -3.1×10^{-16} | 8.1 | 8.5×10^{-29} | ... | 1.0×10^{-25} | 1.1×10^{-6} | 8.3×10^{31} | 1200 |
| J1022+1001 | 60.78 | 121.56 | -1.6×10^{-16} | 0.5 | 2.5×10^{-27} | 4.5×10^{-26} | 4.8×10^{-26} | 1.6×10^{-6} | 1.2×10^{32} | 19 |
| J1024-0719 | 193.72 | 387.43 | 1.3×10^{-16} | 0.5 | 1.3×10^{-27a} | 5.0×10^{-26} | 4.6×10^{-26} | 1.4×10^{-7} | 1.1×10^{31} | 35 |
| J1038+0032 | 34.66 | 69.32 | -7.8×10^{-17} | 2.4 | 5.1×10^{-28} | ... | 1.2×10^{-25} | 5.5×10^{-5} | 4.3×10^{33} | 230 |
| J1045-4509 | 133.79 | 267.59 | -3.1×10^{-16} | 0.2 | 5.3×10^{-27a} | 4.3×10^{-26} | 3.0×10^{-26} | 9.3×10^{-8} | 7.2×10^{30} | 5.7 |
| J1231-1411 | 271.45 | 542.91 | 1.6×10^{-15} | 0.5 | 4.3×10^{-27a} | ... | 7.5×10^{-26} | 1.1×10^{-7} | 8.4×10^{30} | 17 |
| J1300+1240 | 160.81 | 321.62 | -7.9×10^{-16} | 0.6 | 3.0×10^{-27a} | ... | 4.9×10^{-26} | 2.7×10^{-7} | 2.1×10^{31} | 16 |
| J1301+0833 | 542.38 | 1084.76 | -3.1×10^{-15} | 0.9 | 2.1×10^{-27} | ... | 1.1×10^{-25} | 7.9×10^{-8} | 6.1×10^{30} | 51 |
| J1435-6100 ^e | 106.98 | 213.95 | -2.8×10^{-16} | 3.3 | 4.0×10^{-28} | 2.7×10^{-25} | ... | 1.8×10^{-5} | 1.4×10^{33} | 670 |
| J1453+1902 | 172.64 | 345.29 | -3.2×10^{-16} | 0.9 | 1.2×10^{-27a} | ... | 1.4×10^{-25} | 1.0×10^{-6} | 8.0×10^{31} | 120 |
| J1455-3330 | 125.20 | 250.40 | -2.5×10^{-16} | 0.7 | 1.5×10^{-27a} | 5.1×10^{-26} | 3.6×10^{-26} | 4.1×10^{-7} | 3.1×10^{31} | 24 |
| J1518+0204A | 180.06 | 360.13 | -2.9×10^{-15} | 8.0 | 4.0×10^{-28b} | ... | 7.8×10^{-26} | 4.6×10^{-6} | 3.5×10^{32} | 190 |
| J1518+4904 | 24.43 | 48.86 | -1.3×10^{-17} | 0.7 | 8.5×10^{-28a} | ... | 2.9×10^{-25} | 8.1×10^{-5} | 6.2×10^{33} | 340 |
| J1537+1155 | 26.38 | 52.76 | -1.6×10^{-15} | 1.0 | 6.3×10^{-27a} | ... | 2.4×10^{-25} | 8.4×10^{-5} | 6.5×10^{33} | 39 |
| J1600-3053 | 277.94 | 555.88 | -6.5×10^{-16} | 2.4 | 5.1×10^{-28a} | 5.6×10^{-26} | 6.7×10^{-26} | 4.9×10^{-7} | 3.8×10^{31} | 130 |
| J1603-7202 | 67.38 | 134.75 | -5.4×10^{-17} | 1.6 | 4.4×10^{-28a} | 2.3×10^{-26} | 2.3×10^{-26} | 1.9×10^{-6} | 1.5×10^{32} | 51 |
| J1614-2230 | 317.38 | 634.76 | 3.9×10^{-16} | 1.8 | 5.0×10^{-28a} | ... | 6.4×10^{-26} | 2.7×10^{-7} | 2.1×10^{31} | 130 |
| J1623-2631 | 90.29 | 180.57 | -5.1×10^{-15} | 2.2 | 2.7×10^{-27a} | 5.7×10^{-26} | 5.1×10^{-26} | 3.3×10^{-6} | 2.5×10^{32} | 19 |
| J1629-6902 ^e | 166.65 | 333.30 | -2.8×10^{-16} | 1.4 | 7.7×10^{-28} | 3.2×10^{-25} | ... | 3.8×10^{-6} | 2.9×10^{32} | 420 |
| J1630+3734 ^d | 301.38 | 602.75 | -8.9×10^{-16} | 0.9 ^c | 1.5×10^{-27} | ... | 9.0×10^{-26} | 2.2×10^{-7} | 1.7×10^{31} | 60 |
| J1640+2224 | 316.12 | 632.25 | -1.6×10^{-16} | 1.2 | 4.9×10^{-28a} | 6.7×10^{-26} | 5.1×10^{-26} | 1.4×10^{-7} | 1.1×10^{31} | 110 |
| J1641+3627A | 96.36 | 192.72 | -1.5×10^{-15} | 7.5 | 4.3×10^{-28b} | ... | 5.0×10^{-26} | 9.5×10^{-6} | 7.3×10^{32} | 120 |
| J1643-1224 | 216.37 | 432.75 | -8.5×10^{-16} | 0.4 | 3.8×10^{-27a} | 4.4×10^{-26} | 3.6×10^{-26} | 7.6×10^{-8} | 5.9×10^{30} | 9.4 |
| J1701-3006A | 190.78 | 381.57 | -3.0×10^{-15} | 6.9 | 4.7×10^{-28b} | 5.8×10^{-26} | 3.6×10^{-26} | 1.6×10^{-6} | 1.3×10^{32} | 78 |
| J1701-3006B ^f | 278.25 | 556.50 | 2.7×10^{-14} | 6.9 | 4.7×10^{-28b} | 7.6×10^{-26} | ... | 1.6×10^{-6} | 1.2×10^{32} | 160 |
| J1701-3006C ^f | 131.36 | 262.72 | 1.1×10^{-15} | 6.9 | 4.7×10^{-28b} | 3.5×10^{-26} | ... | 3.3×10^{-6} | 2.6×10^{32} | 76 |
| J1709+2313 | 215.93 | 431.85 | -6.9×10^{-17} | 1.8 | 2.5×10^{-28a} | ... | 9.3×10^{-26} | 8.6×10^{-7} | 6.7×10^{31} | 370 |
| J1713+0747 | 218.81 | 437.62 | -3.9×10^{-16} | 1.1 | 1.0×10^{-27a} | 4.5×10^{-26} | 3.5×10^{-26} | 1.8×10^{-7} | 1.4×10^{31} | 34 |
| J1719-1438 | 172.71 | 345.41 | -2.3×10^{-16} | 1.6 | 5.8×10^{-28} | ... | 1.6×10^{-25} | 2.0×10^{-6} | 1.6×10^{32} | 270 |

Table 7
(Continued)

| Pulsar | f_{rot} (Hz) | f_{gw} (Hz) | \dot{f}_{rot} (Hz s ⁻¹) | d (kpc) | h_0^{sd} | Prior $h_0^{95\%}$ | S6/VSR2,4 $h_0^{95\%}$ | ε | Q_{22} (kg m ²) | $h_0^{95\%} / h_0^{\text{sd}}$ |
|---------------------------|--------------------------|-------------------------|---|--------------|-------------------------------|-----------------------|------------------------|----------------------|----------------------------------|--------------------------------|
| J1721–2457 | 285.99 | 571.98 | -2.4×10^{-16} | 1.6 | $4.7 \times 10^{-28\text{a}}$ | ... | 5.5×10^{-26} | 2.5×10^{-7} | 1.9×10^{31} | 120 |
| J1730–2304 | 123.11 | 246.22 | -3.1×10^{-16} | 0.5 | 2.5×10^{-27} | 5.8×10^{-26} | 4.5×10^{-26} | 3.6×10^{-7} | 2.8×10^{31} | 18 |
| J1731–1847 | 426.52 | 853.04 | -4.6×10^{-15} | 4.0 | 6.6×10^{-28} | ... | 1.3×10^{-25} | 6.6×10^{-7} | 5.1×10^{31} | 190 |
| J1732–5049 | 188.23 | 376.47 | -5.0×10^{-16} | 1.8 | 7.3×10^{-28} | 5.3×10^{-26} | 4.6×10^{-26} | 5.6×10^{-7} | 4.3×10^{31} | 63 |
| J1738+0333 | 170.94 | 341.87 | -6.7×10^{-16} | 2.0 | $8.1 \times 10^{-28\text{a}}$ | ... | 1.1×10^{-25} | 1.8×10^{-6} | 1.4×10^{32} | 140 |
| J1741+1351 | 266.87 | 533.74 | -2.2×10^{-15} | 1.4 | 1.6×10^{-27} | ... | 1.1×10^{-25} | 5.1×10^{-7} | 3.9×10^{31} | 67 |
| J1744–1134 | 245.43 | 490.85 | -4.3×10^{-16} | 0.4 | $2.5 \times 10^{-27\text{a}}$ | 1.1×10^{-25} | 6.3×10^{-26} | 1.0×10^{-7} | 8.0×10^{30} | 25 |
| J1745–0952 | 51.61 | 103.22 | -7.6×10^{-17} | 2.4 | $4.1 \times 10^{-28\text{a}}$ | ... | 6.0×10^{-26} | 1.3×10^{-5} | 9.8×10^{32} | 150 |
| J1748–2446A | 86.48 | 172.96 | -1.4×10^{-15} | 5.5 | $5.8 \times 10^{-28\text{b}}$ | 3.9×10^{-26} | 3.2×10^{-26} | 5.6×10^{-6} | 4.3×10^{32} | 55 |
| J1748–2446C | 118.54 | 237.08 | -1.9×10^{-15} | 5.5 | $5.8 \times 10^{-28\text{b}}$ | 5.0×10^{-26} | 3.8×10^{-26} | 3.5×10^{-6} | 2.7×10^{32} | 65 |
| J1748–2446D | 212.14 | 424.27 | -3.4×10^{-15} | 5.5 | $5.8 \times 10^{-28\text{b}}$ | 6.8×10^{-26} | 5.3×10^{-26} | 1.5×10^{-6} | 1.2×10^{32} | 91 |
| J1748–2446E | 455.00 | 910.00 | -7.2×10^{-15} | 5.5 | $5.8 \times 10^{-28\text{b}}$ | 9.0×10^{-26} | 7.3×10^{-26} | 4.6×10^{-7} | 3.6×10^{31} | 130 |
| J1748–2446F | 180.50 | 361.00 | -2.9×10^{-15} | 5.5 | $5.8 \times 10^{-28\text{b}}$ | 8.3×10^{-26} | 7.4×10^{-26} | 3.0×10^{-6} | 2.3×10^{32} | 130 |
| J1748–2446G | 46.14 | 92.29 | -7.3×10^{-16} | 5.5 | $5.8 \times 10^{-28\text{b}}$ | 5.9×10^{-26} | 4.5×10^{-26} | 2.8×10^{-5} | 2.1×10^{33} | 78 |
| J1748–2446H | 203.01 | 406.02 | -3.2×10^{-15} | 5.5 | $5.8 \times 10^{-28\text{b}}$ | 7.8×10^{-26} | 5.8×10^{-26} | 1.8×10^{-6} | 1.4×10^{32} | 99 |
| J1748–2446I | 104.49 | 208.98 | -1.7×10^{-15} | 5.5 | $5.8 \times 10^{-28\text{b}}$ | 3.6×10^{-26} | 3.7×10^{-26} | 4.5×10^{-6} | 3.4×10^{32} | 64 |
| J1748–2446K | 336.74 | 673.48 | -5.3×10^{-15} | 5.5 | $5.8 \times 10^{-28\text{b}}$ | 6.8×10^{-26} | 5.9×10^{-26} | 6.8×10^{-7} | 5.3×10^{31} | 100 |
| J1748–2446L | 445.49 | 890.99 | -7.1×10^{-15} | 5.5 | $5.8 \times 10^{-28\text{b}}$ | 1.4×10^{-25} | 1.1×10^{-25} | 7.5×10^{-7} | 5.8×10^{31} | 200 |
| J1748–2446M | 280.15 | 560.29 | -4.4×10^{-15} | 5.5 | $5.8 \times 10^{-28\text{b}}$ | 1.0×10^{-25} | 9.5×10^{-26} | 1.6×10^{-6} | 1.2×10^{32} | 160 |
| J1748–2446N | 115.38 | 230.76 | -1.8×10^{-15} | 5.5 | $5.8 \times 10^{-28\text{b}}$ | 5.8×10^{-26} | 6.4×10^{-26} | 6.3×10^{-6} | 4.8×10^{32} | 110 |
| J1748–2446O | 596.44 | 1192.87 | -9.4×10^{-15} | 5.5 | $5.8 \times 10^{-28\text{b}}$ | 2.6×10^{-25} | 2.6×10^{-25} | 9.6×10^{-7} | 7.4×10^{31} | 450 |
| J1748–2446P ^f | 578.50 | 1157.00 | -8.7×10^{-14} | 5.5 | $5.8 \times 10^{-28\text{b}}$ | 1.6×10^{-25} | ... | 6.1×10^{-7} | 4.8×10^{31} | 267 |
| J1748–2446Q | 355.64 | 711.29 | -5.6×10^{-15} | 5.5 | $5.8 \times 10^{-28\text{b}}$ | 8.8×10^{-26} | 9.4×10^{-26} | 9.7×10^{-7} | 7.5×10^{31} | 160 |
| J1748–2446R | 198.86 | 397.73 | -3.2×10^{-15} | 5.5 | $5.8 \times 10^{-28\text{b}}$ | 8.1×10^{-26} | 5.1×10^{-26} | 1.7×10^{-6} | 1.3×10^{32} | 87 |
| J1748–2446S | 163.49 | 326.98 | -2.6×10^{-15} | 5.5 | $5.8 \times 10^{-28\text{b}}$ | 4.5×10^{-26} | 5.3×10^{-26} | 2.6×10^{-6} | 2.0×10^{32} | 91 |
| J1748–2446T | 141.15 | 282.29 | -2.2×10^{-15} | 5.5 | $5.8 \times 10^{-28\text{b}}$ | 5.1×10^{-26} | 3.0×10^{-26} | 2.0×10^{-6} | 1.5×10^{32} | 52 |
| J1748–2446U | 304.03 | 608.06 | -4.8×10^{-15} | 5.5 | $5.8 \times 10^{-28\text{b}}$ | ... | 1.4×10^{-25} | 1.9×10^{-6} | 1.5×10^{32} | 230 |
| J1748–2446V | 482.51 | 965.02 | -7.6×10^{-15} | 5.5 | $5.8 \times 10^{-28\text{b}}$ | 1.3×10^{-25} | 1.3×10^{-25} | 7.2×10^{-7} | 5.6×10^{31} | 220 |
| J1748–2446W | 237.80 | 475.60 | -3.8×10^{-15} | 5.5 | $5.8 \times 10^{-28\text{b}}$ | 9.4×10^{-26} | 9.5×10^{-26} | 2.2×10^{-6} | 1.7×10^{32} | 160 |
| J1748–2446X | 333.42 | 666.83 | -5.3×10^{-15} | 5.5 | $5.8 \times 10^{-28\text{b}}$ | 8.3×10^{-26} | 4.8×10^{-26} | 5.7×10^{-7} | 4.4×10^{31} | 83 |
| J1748–2446Y | 488.24 | 976.49 | -7.7×10^{-15} | 5.5 | $5.8 \times 10^{-28\text{b}}$ | 2.1×10^{-25} | 2.1×10^{-25} | 1.2×10^{-6} | 9.0×10^{31} | 370 |
| J1748–2446Z | 406.08 | 812.15 | -6.4×10^{-15} | 5.5 | $5.8 \times 10^{-28\text{b}}$ | 8.5×10^{-26} | 8.6×10^{-26} | 6.8×10^{-7} | 5.2×10^{31} | 150 |
| J1748–2446aa | 172.77 | 345.54 | -2.7×10^{-15} | 5.5 | $5.8 \times 10^{-28\text{b}}$ | 2.3×10^{-25} | 1.5×10^{-25} | 6.6×10^{-6} | 5.1×10^{32} | 260 |
| J1748–2446ab | 195.32 | 390.65 | -3.1×10^{-15} | 5.5 | $5.8 \times 10^{-28\text{b}}$ | 4.7×10^{-26} | 4.0×10^{-26} | 1.4×10^{-6} | 1.1×10^{32} | 69 |
| J1748–2446ac | 196.58 | 393.17 | -3.1×10^{-15} | 5.5 | $5.8 \times 10^{-28\text{b}}$ | 7.2×10^{-26} | 5.6×10^{-26} | 1.9×10^{-6} | 1.5×10^{32} | 97 |
| J1748–2446ad ^f | 716.36 | 1432.70 | 1.7×10^{-14} | 5.5 | $5.8 \times 10^{-28\text{b}}$ | 1.8×10^{-25} | ... | 4.5×10^{-7} | 3.5×10^{31} | 300 |
| J1748–2446ae | 273.33 | 546.66 | -4.3×10^{-15} | 5.5 | $5.8 \times 10^{-28\text{b}}$ | 6.6×10^{-26} | 6.8×10^{-26} | 1.2×10^{-6} | 9.2×10^{31} | 120 |
| J1748–2446af | 302.63 | 605.26 | -4.8×10^{-15} | 5.5 | $5.8 \times 10^{-28\text{b}}$ | 1.1×10^{-25} | 6.0×10^{-26} | 8.5×10^{-7} | 6.5×10^{31} | 100 |
| J1748–2446ag | 224.82 | 449.64 | -3.6×10^{-15} | 5.5 | $5.8 \times 10^{-28\text{b}}$ | 9.4×10^{-26} | 5.1×10^{-26} | 1.3×10^{-6} | 1.0×10^{32} | 87 |
| J1748–2446ah | 201.40 | 402.81 | -3.2×10^{-15} | 5.5 | $5.8 \times 10^{-28\text{b}}$ | 5.5×10^{-26} | 4.0×10^{-26} | 1.3×10^{-6} | 10.0×10^{31} | 69 |
| J1748–2446ai | 47.11 | 94.21 | -7.5×10^{-16} | 5.5 | $5.8 \times 10^{-28\text{b}}$ | ... | 1.6×10^{-25} | 9.2×10^{-5} | 7.1×10^{33} | 270 |
| J1751–2857 | 255.44 | 510.87 | -7.3×10^{-16} | 1.4 | 9.5×10^{-28} | ... | 6.8×10^{-26} | 3.6×10^{-7} | 2.8×10^{31} | 72 |
| J1756–2251 | 35.14 | 70.27 | -1.3×10^{-15} | 2.9 | 1.7×10^{-27} | 9.7×10^{-26} | 7.4×10^{-26} | 4.1×10^{-5} | 3.2×10^{33} | 45 |
| J1757–5322 ^e | 112.74 | 225.48 | -3.3×10^{-16} | 1.4 | 1.0×10^{-27} | 3.7×10^{-25} | ... | 9.4×10^{-6} | 7.3×10^{32} | 360 |
| J1801–1417 | 275.85 | 551.71 | 3.1×10^{-16} | 1.8 | $4.8 \times 10^{-28\text{a}}$ | 6.2×10^{-26} | 7.3×10^{-26} | 4.1×10^{-7} | 3.1×10^{31} | 150 |
| J1801–3210 | 134.16 | 268.33 | 1.8×10^{-17} | 5.0 | 5.8×10^{-29} | ... | 3.5×10^{-26} | 2.3×10^{-6} | 1.8×10^{32} | 610 |
| J1802–2124 | 79.07 | 158.13 | -4.4×10^{-16} | 3.3 | $5.7 \times 10^{-28\text{a}}$ | ... | 4.7×10^{-26} | 6.0×10^{-6} | 4.6×10^{32} | 83 |
| J1803–30 | 140.82 | 281.63 | -2.2×10^{-15} | 7.8 | $4.1 \times 10^{-28\text{b}}$ | 5.5×10^{-26} | 4.1×10^{-26} | 3.8×10^{-6} | 3.0×10^{32} | 100 |
| J1804–0735 | 43.29 | 86.58 | -6.9×10^{-16} | 8.4 | $3.8 \times 10^{-28\text{b}}$ | 8.4×10^{-26} | 8.8×10^{-26} | 9.4×10^{-5} | 7.2×10^{33} | 230 |
| J1804–2717 | 107.03 | 214.06 | -4.7×10^{-16} | 1.2 | 1.4×10^{-27} | 2.4×10^{-26} | 2.2×10^{-26} | 5.3×10^{-7} | 4.1×10^{31} | 15 |
| J1807–2459A | 326.86 | 653.71 | -5.2×10^{-15} | 2.7 | $1.2 \times 10^{-27\text{b}}$ | 1.5×10^{-25} | 9.6×10^{-26} | 5.8×10^{-7} | 4.5×10^{31} | 81 |
| J1810+1744 | 601.41 | 1202.82 | -1.6×10^{-15} | 2.5 | 5.3×10^{-28} | ... | 1.8×10^{-25} | 2.9×10^{-7} | 2.3×10^{31} | 340 |
| J1810–2005 | 30.47 | 60.93 | -5.0×10^{-17} | 4.0 | $2.6 \times 10^{-28\text{a}}$ | 2.2×10^{-25} | 1.6×10^{-25} | 1.6×10^{-4} | 1.3×10^{34} | 630 |
| J1811–2405 | 375.86 | 751.71 | -1.9×10^{-15} | 1.7 | 1.1×10^{-27} | ... | 8.5×10^{-26} | 2.4×10^{-7} | 1.9×10^{31} | 80 |
| J1823–3021A | 183.82 | 367.65 | -2.9×10^{-15} | 7.9 | $4.1 \times 10^{-28\text{b}}$ | 4.0×10^{-26} | 3.5×10^{-26} | 1.9×10^{-6} | 1.5×10^{32} | 86 |
| J1824–2452A | 327.41 | 654.81 | -1.7×10^{-13} | 5.5 | $3.4 \times 10^{-27\text{a}}$ | 7.9×10^{-26} | 5.5×10^{-26} | 6.7×10^{-7} | 5.2×10^{31} | 16 |
| J1824–2452B ^f | 152.75 | 305.50 | 5.6×10^{-15} | 5.5 | $5.8 \times 10^{-28\text{b}}$ | 4.2×10^{-26} | ... | 2.3×10^{-6} | 1.8×10^{32} | 72 |
| J1824–2452C ^f | 240.48 | 480.96 | -9.8×10^{-15} | 5.5 | $5.8 \times 10^{-28\text{b}}$ | 6.6×10^{-26} | ... | 1.5×10^{-6} | 1.2×10^{32} | 110 |
| J1824–2452E ^f | 184.53 | 369.06 | 3.7×10^{-15} | 5.5 | $5.8 \times 10^{-28\text{b}}$ | 7.5×10^{-26} | ... | 2.9×10^{-6} | 2.2×10^{32} | 130 |
| J1824–2452F ^f | 407.97 | 815.94 | -1.6×10^{-15} | 5.5 | $5.8 \times 10^{-28\text{b}}$ | 9.8×10^{-26} | ... | 7.6×10^{-7} | 5.9×10^{31} | 170 |
| J1824–2452G ^f | 169.23 | 338.46 | -5.2×10^{-15} | 5.5 | $5.8 \times 10^{-28\text{b}}$ | 7.3×10^{-26} | ... | 3.3×10^{-6} | 2.6×10^{32} | 130 |
| J1824–2452H ^f | 216.01 | 432.02 | -3.6×10^{-15} | 5.5 | $5.8 \times 10^{-28\text{b}}$ | 8.2×10^{-26} | ... | 2.3×10^{-6} | 1.8×10^{32} | 140 |
| J1824–2452I ^g | 254.33 | 508.67 | -5.4×10^{-15} | 5.5 | $5.8 \times 10^{-28\text{b}}$ | 2.2×10^{-25} | ... | 4.4×10^{-6} | 3.4×10^{32} | 370 |
| J1824–2452J ^f | 247.54 | 495.08 | 4.7×10^{-15} | 5.5 | $5.8 \times 10^{-28\text{b}}$ | 1.1×10^{-25} | ... | 2.3×10^{-6} | 1.7×10^{32} | 180 |
| J1841+0130 | 33.59 | 67.18 | -9.2×10^{-15} | 3.2 | 4.2×10^{-27} | 1.6×10^{-25} | 1.3×10^{-25} | 8.7×10^{-5} | 6.7×10^{33} | 31 |

Table 7
(Continued)

| Pulsar | f_{rot} (Hz) | f_{gw} (Hz) | \dot{f}_{rot} (Hz s ⁻¹) | d (kpc) | h_0^{sd} | Prior $h_0^{95\%}$ | S6/VSR2,4 $h_0^{95\%}$ | ε | Q_{22} (kg m ²) | $h_0^{95\%} / h_0^{\text{sd}}$ |
|--------------------------|--------------------------|-------------------------|---|--------------|------------------------|-----------------------|------------------------|----------------------|----------------------------------|--------------------------------|
| J1843–1113 | 541.81 | 1083.62 | -2.8×10^{-15} | 2.0 | 9.3×10^{-28} | 1.6×10^{-25} | 1.1×10^{-25} | 1.8×10^{-7} | 1.4×10^{31} | 120 |
| J1853+1303 | 244.39 | 488.78 | -5.1×10^{-16} | 1.6 | 7.3×10^{-28a} | ... | 8.5×10^{-26} | 5.4×10^{-7} | 4.2×10^{31} | 120 |
| J1857+0943 | 186.49 | 372.99 | -6.1×10^{-16} | 0.9 | 1.6×10^{-27a} | 7.3×10^{-26} | 5.7×10^{-26} | 3.5×10^{-7} | 2.7×10^{31} | 35 |
| J1903+0327 | 465.14 | 930.27 | -3.8×10^{-15} | 6.5 | 3.6×10^{-28a} | ... | 1.6×10^{-25} | 1.1×10^{-6} | 8.8×10^{31} | 450 |
| J1905+0400 | 264.24 | 528.48 | -2.8×10^{-16} | 1.3 | 6.3×10^{-28a} | 7.4×10^{-26} | 5.0×10^{-26} | 2.3×10^{-7} | 1.8×10^{31} | 80 |
| J1909–3744 | 339.32 | 678.63 | -1.9×10^{-16} | 1.3 | 4.7×10^{-28a} | 8.2×10^{-26} | 5.9×10^{-26} | 1.5×10^{-7} | 1.2×10^{31} | 120 |
| J1910+1256 | 200.66 | 401.32 | -3.4×10^{-16} | 1.9 | 5.4×10^{-28a} | ... | 7.7×10^{-26} | 8.8×10^{-7} | 6.8×10^{31} | 140 |
| J1910–5959A | 306.17 | 612.33 | -1.9×10^{-16} | 4.5 | 1.4×10^{-28a} | 7.7×10^{-26} | 5.5×10^{-26} | 6.2×10^{-7} | 4.8×10^{31} | 390 |
| J1910–5959B | 119.65 | 239.30 | -1.9×10^{-15} | 4.5 | 7.1×10^{-28b} | 3.8×10^{-26} | 2.5×10^{-26} | 1.9×10^{-6} | 1.4×10^{32} | 35 |
| J1910–5959C | 189.49 | 378.98 | 1.1×10^{-18} | 4.5 | 1.4×10^{-29a} | 4.4×10^{-26} | 3.2×10^{-26} | 9.5×10^{-7} | 7.4×10^{31} | 2300 |
| J1910–5959D | 110.68 | 221.35 | -1.8×10^{-15} | 4.5 | 7.1×10^{-28b} | 3.1×10^{-26} | 2.1×10^{-26} | 1.8×10^{-6} | 1.4×10^{32} | 29 |
| J1910–5959E | 218.73 | 437.47 | -3.5×10^{-15} | 4.5 | 7.1×10^{-28b} | 4.8×10^{-26} | 3.6×10^{-26} | 8.0×10^{-7} | 6.1×10^{31} | 50 |
| J1911+0101A ^e | 276.36 | 552.71 | 5.0×10^{-16} | 7.4 | 4.3×10^{-28b} | 6.0×10^{-25} | ... | 1.4×10^{-5} | 1.1×10^{33} | 1400 |
| J1911+0101B ^e | 185.72 | 371.45 | 6.9×10^{-17} | 7.4 | 4.3×10^{-28b} | 7.4×10^{-25} | ... | 3.8×10^{-5} | 2.9×10^{33} | 1700 |
| J1911+1347 | 216.17 | 432.34 | -7.9×10^{-16} | 1.6 | 9.6×10^{-28} | 7.0×10^{-26} | 4.8×10^{-26} | 3.9×10^{-7} | 3.0×10^{31} | 50 |
| J1911–1114 | 275.81 | 551.61 | -4.7×10^{-16} | 1.6 | 6.7×10^{-28a} | 5.7×10^{-26} | 6.3×10^{-26} | 3.1×10^{-7} | 2.4×10^{31} | 94 |
| J1918–0642 | 130.79 | 261.58 | -4.0×10^{-16} | 1.4 | 1.0×10^{-27a} | ... | 4.0×10^{-26} | 7.7×10^{-7} | 6.0×10^{31} | 39 |
| J1939+2134 | 641.93 | 1283.86 | -4.3×10^{-14} | 5.0 | 1.3×10^{-27a} | 1.8×10^{-25} | 1.3×10^{-25} | 3.6×10^{-7} | 2.8×10^{31} | 96 |
| J1944+0907 | 192.86 | 385.71 | -3.6×10^{-16} | 1.3 | 8.6×10^{-28a} | ... | 5.5×10^{-26} | 4.4×10^{-7} | 3.4×10^{31} | 64 |
| J1955+2908 | 163.05 | 326.10 | -7.5×10^{-16} | 5.4 | 3.2×10^{-28a} | 7.0×10^{-26} | 5.4×10^{-26} | 2.6×10^{-6} | 2.0×10^{32} | 170 |
| J1959+2048 | 622.12 | 1244.24 | -4.4×10^{-15} | 1.5 | 1.4×10^{-27a} | ... | 1.5×10^{-25} | 1.4×10^{-7} | 1.1×10^{31} | 110 |
| J2007+2722 | 40.82 | 81.64 | -1.6×10^{-15} | 6.8 | 7.4×10^{-28} | ... | 7.1×10^{-26} | 6.9×10^{-5} | 5.3×10^{33} | 96 |
| J2010–1323 | 191.45 | 382.90 | -1.8×10^{-16} | 1.3 | 6.0×10^{-28} | ... | 6.3×10^{-26} | 5.2×10^{-7} | 4.0×10^{31} | 100 |
| J2017+0603 | 345.28 | 690.56 | -9.6×10^{-16} | 1.3 | 1.0×10^{-27} | ... | 1.3×10^{-25} | 3.4×10^{-7} | 2.6×10^{31} | 130 |
| J2019+2425 | 254.16 | 508.32 | -1.7×10^{-16} | 0.9 | 7.2×10^{-28a} | 9.2×10^{-26} | 5.6×10^{-26} | 1.9×10^{-7} | 1.4×10^{31} | 79 |
| J2033+17 | 168.10 | 336.19 | -2.3×10^{-16} | 1.4 | 6.8×10^{-28a} | 7.5×10^{-26} | 8.0×10^{-26} | 9.2×10^{-7} | 7.1×10^{31} | 120 |
| J2043+1711 | 420.19 | 840.38 | -7.3×10^{-16} | 1.1 | 9.4×10^{-28a} | ... | 7.3×10^{-26} | 1.1×10^{-7} | 8.5×10^{30} | 78 |
| J2051–0827 | 221.80 | 443.59 | -6.1×10^{-16} | 1.3 | 1.0×10^{-27a} | 7.5×10^{-26} | 5.3×10^{-26} | 3.3×10^{-7} | 2.5×10^{31} | 51 |
| J2124–3358 | 202.79 | 405.59 | -4.4×10^{-16} | 0.3 | 4.0×10^{-27a} | 4.9×10^{-26} | 3.9×10^{-26} | 6.7×10^{-8} | 5.2×10^{30} | 9.9 |
| J2129–5721 | 268.36 | 536.72 | -1.5×10^{-15} | 0.4 | 4.7×10^{-27a} | 6.2×10^{-26} | 5.2×10^{-26} | 6.8×10^{-8} | 5.3×10^{30} | 11 |
| J2140–2310A | 90.75 | 181.50 | -1.4×10^{-15} | 9.2 | 3.5×10^{-28b} | ... | 5.9×10^{-26} | 1.6×10^{-5} | 1.2×10^{33} | 170 |
| J2145–0750 | 62.30 | 124.59 | -1.0×10^{-16} | 0.6 | 1.8×10^{-27a} | 3.8×10^{-26} | 2.9×10^{-26} | 1.4×10^{-6} | 7.9×10^{31} | 16 |
| J2214+3000 | 320.59 | 641.18 | -1.5×10^{-15} | 1.3 | 1.3×10^{-27} | ... | 7.2×10^{-26} | 2.2×10^{-7} | 1.7×10^{31} | 54 |
| J2215+5135 | 383.20 | 766.40 | -4.1×10^{-15} | 3.3 | 8.0×10^{-28} | ... | 1.6×10^{-25} | 8.7×10^{-7} | 6.7×10^{31} | 200 |
| J2229+2643 | 335.82 | 671.63 | 1.7×10^{-16} | 1.4 | 4.1×10^{-28a} | 9.9×10^{-26} | 6.5×10^{-26} | 2.0×10^{-7} | 1.5×10^{31} | 160 |
| J2241–5236 | 457.31 | 914.62 | -1.4×10^{-15} | 0.7 | 2.1×10^{-27} | ... | 8.9×10^{-26} | 6.9×10^{-8} | 5.3×10^{30} | 42 |
| J2302+4442 | 192.59 | 385.18 | -5.1×10^{-16} | 0.8 | 1.8×10^{-27} | ... | 4.5×10^{-26} | 2.2×10^{-7} | 1.7×10^{31} | 26 |
| J2317+1439 | 290.25 | 580.51 | -1.3×10^{-16} | 1.9 | 2.8×10^{-28a} | 8.8×10^{-26} | 5.6×10^{-26} | 3.0×10^{-7} | 2.3×10^{31} | 200 |
| J2322+2057 | 207.97 | 415.94 | -1.8×10^{-16} | 0.8 | 9.6×10^{-28a} | 1.1×10^{-25} | 5.4×10^{-26} | 2.3×10^{-7} | 1.8×10^{31} | 57 |

Notes. Detector calibration errors mean that for pulsars with f_{gw} below and above 50 Hz there are $\sim 6\%$ and $\sim 20\%$ uncertainties on these limits respectively.

^a The pulsar's spin-down is corrected for proper motion effects.

^b The pulsar's spin-down is calculated using a characteristic spin-down age of 10^9 yr.

^c The pulsar's distance is calculated using the NE2001 model of Cordes & Lazio (2002).

^d Recently discovered pulsar with timing solution from after the end of S6 or VSR4. As this is an MSP the timing solution should extrapolate back well over the search period and it is unlikely that any glitches occurred.

^e Results from S3/S4 (Abbott et al. 2007a).

^f Results from S5 (Abbott et al. 2010).

^g New result from S5 using data covering 2006.

quadrupole limits are generally within 10^{34} – 10^{35} kg m², with the Crab pulsar upper limit slightly lower at $\sim 7 \times 10^{33}$ kg m². Therefore, for these stars to emit gravitational waves at current sensitivities the emission would most likely have to come from a quark star or one with a hybrid core, whilst the Crab pulsar is about an order of magnitude above the maximum quadrupoles expected for purely crustal emission. However, for advanced detectors the sensitivity for Crab pulsar would be consistent with most optimistic predictions for *normal* neutron stars. For J0537–6910, which has a quadrupole limit close to the Crab pulsar, future prospects may not be so good for reaching the most optimistic prediction for *normal* neutron

stars. This is due to the requirement for phase coherent timing, which for these analyses relied on the no-longer-operational *RXTE*.

For the Crab and Vela pulsars, our results now limit the gravitational wave emission to contribute $\lesssim 1\%$ and $\lesssim 10\%$ of their respective spin-down luminosities, with an improvement of about a factor of 4 for Vela with respect to previous results. These limits are compatible with the observed braking indices of the pulsars, which are $n = 2.51$ and $n \approx 1.4$ respectively (see, e.g., Palomba 2000).

Given various assumptions about the magnetic field discussed above, our results constrain the internal field of the Crab

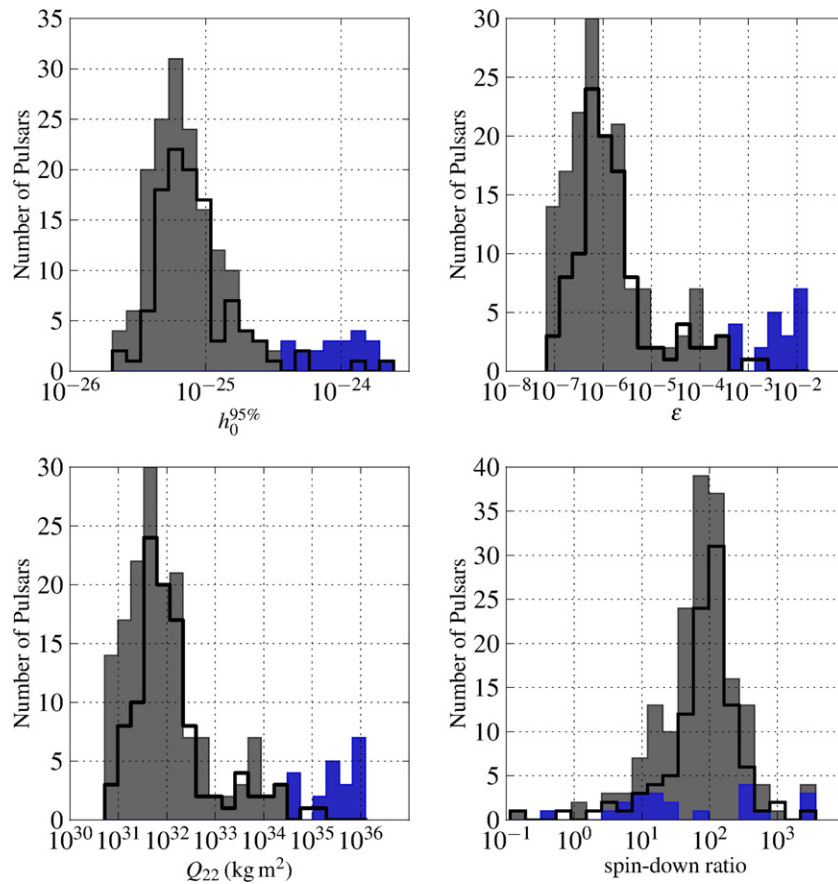


Figure 3. Upper limits in histogram form for all pulsars for h_0 , ϵ , Q_{22} and the spin-down limit ratio. The gray shaded area represents results from the S6/VSR2.4 analysis combining all detectors, the blue shaded area represents results from the VSR2.4-only analyses. These also contain the seven high interest pulsars for which the Bayesian method values have been plotted based on no assumptions about the pulsar orientations. Previous upper limits from the S5 analysis are given by the unfilled histogram.

(A color version of this figure is available in the online journal.)

pulsar to be less than $\sim 10^{16}$ G (e.g., Cutler 2002). For the other high interest pulsars, the limits on the magnetic field would be even higher than this, so we have not included them here.

Johnson-McDaniel (2013) relates the limits on the $l = m = 2$ quadrupole moment from the gravitational wave emission to the physical surface deformation of a star for a variety of equations of state, which can be compared to the oblateness due to rotation (note that there is no particular reason to expect a relation between these quantities). His results showed that previous gravitational wave limits for the Crab pulsar constrained the surface deformation from the $l = m = 2$ quadrupole to be well below the rotational deformation for all equations of state and neutron star masses. Our new results slightly improve these limits, with the physical surface deformation limited to less than ~ 30 cm, maximized over masses and equations of state. For the Vela pulsar, our new results limit non-axisymmetric quadrupole deformations to be $\lesssim 100$ cm, which is smaller than the expected rotational oblateness for equations of state with large radii.

For PSR J0537–6910, the quality of S6 data at the corresponding frequency was relatively poor, and the upper limits are no better than those produced during S5 (Abbott et al. 2010). If this pulsar were, however, at the upper end of the moment of inertia range ($\sim 3 \times 10^{38}$ kg m²) the spin-down limit

would be increased by a factor of ~ 1.7 , and we would now fall below it.¹⁵⁵

4.3. Other Highlights

Several other pulsar upper limits are within a factor of 10 of their spin-down limits. For the MSPs, three upper limits are within a factor of ten of the spin-down limit: J1045–4509, a factor of 6; J1643–1224, a factor of 10; and J2124–3358, also a factor of 10. The upper limit that corresponds to the smallest ellipticity/mass quadrupole is from J2124–3358 with $\epsilon = 6.7 \times 10^{-8}$ and $Q_{22} = 5.2 \times 10^{30}$ kg m². Although this value is currently above the spin-down limit, it is well within allowable maximum deformations for all neutron star equations of state (see, e.g., Pitkin 2011). The gravitational wave spin-down limits for these pulsars require quadrupoles that are well within reasonable theoretical ranges, so they will make intriguing targets for the advanced generation of detectors.

For the young pulsars only targeted with Virgo VSR2 and VSR4 data a further five are within a factor of 10 of the spin-down limit (see Table 6). All of these would be required to have an exotic equation of state to be observed at around their spin-down limits in future detectors.

¹⁵⁵ The distance to the Large Magellanic Cloud is known to $\sim 2\%$ (Pietrzyński et al. 2013), so does not significantly contribute to the uncertainty on the spin-down limit.

Table 8
RXTE Ephemerides for J0537–6910 During the Period of S6, VSR2, and VSR4

| EM Observation Span (MJD and Date) | Epoch t_0 (MJD _{TDB}) | f_{rot} (Hz) | \dot{f}_{rot} (10^{-10} Hz s $^{-1}$) | \ddot{f}_{rot} (10^{-20} Hz s $^{-2}$) |
|--|--------------------------------------|--------------------------|---|--|
| 54897 (2009 Mar 7) – 55041 (2009 Jul 29) | 54966.4266616022 | 61.9765822442 | –1.9948300 | 0.960 |
| 55045 (2009 Aug 2) – 55182 (2009 Dec 17) | 55140.0377727133 | 61.9736036203 | –1.9939924 | 2.090 |
| 55185 (2009 Dec 20) – 55263 (2010 Mar 8) | 55221.0562912318 | 61.9722204755 | –1.9951973 | 2.090 |
| 55275 (2010 Mar 20) – 55445 (2010 Sep 6) | 55313.6488838244 | 61.9706584446 | –1.9953330 | 0.673 |
| 55458 (2010 Sep 19) – 55503 (2010 Nov 3) | 55475.6859208615 | 61.9678758925 | –1.9952574 | 0.673 |

4.4. Future Prospects

The search results described in this paper assume that the pulsar gravitational-wave phase evolution is very well known and tied very closely to the observed electromagnetic phase. However, precession (e.g., Zimmermann & Szedenits 1979; Jones & Andersson 2002) or other models (Jones 2010) could give emission at both the rotation frequency and twice the rotation frequency. Additionally, as discussed in Abbott et al. (2008), emission may be offset from the electromagnetic phase model. We therefore will be applying methods to search for gravitational waves from known pulsars at multiple harmonics and with narrow bandwidths around the observed electromagnetic values in archival and future datasets.

We look forward to the era of the *advanced* LIGO (aLIGO) (Harry & LIGO Scientific Collaboration 2010) and Virgo (AdV) (Acernese et al. 2009; Accadia et al. 2012) detectors (see Aasi et al. 2013c, for estimates of the aLIGO and AdV observation schedule and sensitivity evolution), as well as the KAGRA detector (Somiya 2012). Ongoing radio pulsar surveys are discovering new objects that will be targeted with future detectors. Currently, the High Time Resolution Universe survey with the Parkes and Effelsberg telescopes (Keith et al. 2010) has discovered 29 new MSPs (Keith 2013; Ng et al. 2013) and could discover up to ~ 75 once complete. The high sensitivity Arecibo PALFA survey is discovering new pulsars (Lazarus 2013) and making use of distributed computing through Einstein@home (Allen et al. 2013). The Green Bank Drift-scan survey and the Green Bank North Celestial Cap survey are also discovering new and interesting sources (Lynch et al. 2013). Many interesting high energy pulsars, undetectable in the radio frequency band, are also being detected by the *Fermi* LAT (Saz Parkinson et al. 2013). *Fermi* is also providing targets to facilitate radio searches which are finding many new MSPs. In addition, new analyses of archive data, such as using Einstein@home to search through Parkes Multi-beam Pulsar Survey data, are still yielding new results (Knispel et al. 2013). In the near future, there are exciting prospects from the Low Frequency Array, which could detect the majority of radio pulsars within ~ 2 kpc, giving of order 1000 new pulsars (van Leeuwen & Stappers 2010; Stappers et al. 2011), and perform deep searches for pulsars in globular clusters.

Finally, we should emphasize that known pulsar searches are not the only searches looking for gravitational waves from rotating, galactic neutron stars. There have been, or are under way, several directed searches looking for sources of unknown frequency and spin-down in particular objects, e.g., globular clusters, supernova remnants (e.g., Abadie et al. 2010; Chung et al. 2011), the Galactic center (Aasi et al. 2013a), and low-mass X-ray binaries. There are also several semi-coherent, all-sky, wide-frequency band searches (e.g., Abadie et al. 2012; Aasi et al. 2013b). Very similar pipelines will be used during the advanced detector era, yielding signal

candidates, performing follow-ups and, in case of detection, source parameter estimation.

The authors gratefully acknowledge the support of the United States National Science Foundation for the construction and operation of the LIGO Laboratory, the Science and Technology Facilities Council of the United Kingdom, the Max-Planck-Society, and the State of Niedersachsen/Germany for support of the construction and operation of the GEO600 detector, and the Italian Istituto Nazionale di Fisica Nucleare and the French Centre National de la Recherche Scientifique for the construction and operation of the Virgo detector. The authors also gratefully acknowledge the support of the research by these agencies and by the Australian Research Council, the International Science Linkages program of the Commonwealth of Australia, the Council of Scientific and Industrial Research of India, the Istituto Nazionale di Fisica Nucleare of Italy, the Spanish Ministerio de Economía y Competitividad, the Conselleria d’Economia Hisenda i Innovació of the Govern de les Illes Balears, the Foundation for Fundamental Research on Matter supported by the Netherlands Organisation for Scientific Research, the Polish Ministry of Science and Higher Education, the FOCUS Programme of Foundation for Polish Science, the Royal Society, the Scottish Funding Council, the Scottish Universities Physics Alliance, the National Aeronautics and Space Administration, OTKA of Hungary, the Lyon Institute of Origins (LIO), the National Research Foundation of Korea, Industry Canada and the Province of Ontario through the Ministry of Economic Development and Innovation, the National Science and Engineering Research Council Canada, the Carnegie Trust, the Leverhulme Trust, the David and Lucile Packard Foundation, the Research Corporation, and the Alfred P. Sloan Foundation. The Nançay Radio Observatory is operated by the Paris Observatory, associated with the French Centre National de la Recherche Scientifique. LIGO Document No. LIGO-P1200104.

APPENDIX

EPHEMERIS FOR J0537–6910

Over the span of S6, VSR2, and VSR4 *RXTE* made observations of J0537–6910. It was observed to glitch four times during this period and phase connected ephemerides were produced for each inter-glitch segment. These ephemerides, given in Table 8, use a DE200 sky position of $\alpha = 05^{\text{h}}37^{\text{m}}47^{\text{s}}.36$ and $\delta = -69^{\circ}10'20''.4$ (Wang et al. 2001).

REFERENCES

- Aasi, J., Abadie, J., Abbott, B. P., et al. 2012, *CQGra*, **29**, 155002
Aasi, J., Abadie, J., Abbott, B. P., et al. 2013a, *PhRvD*, **88**, 102002
Aasi, J., Abadie, J., Abbott, B. P., et al. 2013b, *PhRvD*, **87**, 042001
Aasi, J., Abadie, J., Abbott, B. P., et al. 2013c, arXiv:1304.0670
Abadie, J., Abbott, B. P., Abbott, R., et al. 2010, *ApJ*, **722**, 1504
Abadie, J., Abbott, B. P., Abbott, R., et al. 2011, *ApJ*, **737**, 93

- Abadie, J., Abbott, B. P., Abbott, R., et al. 2012, *PhRvD*, **85**, 022001
- Abbott, B., Abbott, R., Adhikari, R., et al. 2004, *PhRvD*, **69**, 082004
- Abbott, B., Abbott, R., Adhikari, R., et al. 2005, *PhRvL*, **94**, 181103
- Abbott, B., Abbott, R., Adhikari, R., et al. 2007a, *PhRvD*, **76**, 042001
- Abbott, B., Abbott, R., Adhikari, R., et al. 2007b, *PhRvD*, **76**, 082001
- Abbott, B., Abbott, R., Adhikari, R., et al. 2008, *ApJL*, **683**, L45
- Abbott, B. P., Abbott, R., Adhikari, R., et al. 2009, *RPPh*, **72**, 076901
- Abbott, B. P., Abbott, R., Acernese, F., et al. 2010, *ApJ*, **713**, 671
- Abdo, A. A., Ackermann, M., Ajello, M., et al. 2009, *Sci*, **325**, 840
- Accadia, T., Acernese, F., Agathos, M., et al. 2012, Advanced Virgo Technical Design Report, Tech. Rep. VIR-0128A-12, <https://tds.ego-gw.it/ql/?c=8940>
- Accadia, T., Acernese, F., Antonucci, F., et al. 2011, *CQGra*, **28**, 025005
- Acernese, F., Alshourbagy, M., Antonucci, F., et al. 2009, Advanced Virgo Baseline Design, Tech. Rep. VIR-0027A-09, <https://tds.ego-gw.it/ql/?c=6589>
- Adhikari, R., Fritschel, P., & Waldman, S. 2006, Enhanced LIGO, Tech. Rep. LIGO-T060156-v01, California Institute of Technology, Massachusetts Institute of Technology, <https://dcc.ligo.org/LIGO-T060156-v1/public>
- Akgun, T., & Wasserman, I. 2007, *MNRAS*, **383**, 1551
- Allen, B., Knispel, B., Cordes, J. M., et al. 2013, *ApJ*, **773**, 91
- Astone, P., Colla, A., D'Antonio, S., Frasca, S., & Palomba, C. 2012, *JPhCS*, **363**, 012038
- Astone, P., D'Antonio, S., Frasca, S., & Palomba, C. 2010, *CQGra*, **27**, 194016
- Bartos, I., Belopolski, I., Berliner, J., et al. 2011, Frequency Domain Calibration Error Budget for LIGO in S6, Tech. Rep. LIGO-T1100071-v9, LIGO Laboratory, <https://dcc.ligo.org/LIGO-T1100071-v9/public>
- Bonazzola, S., & Gourgoulhon, E. 1996, *A&A*, **312**, 675
- Brooks, S. P., & Roberts, G. O. 1998, *Statistics and Computing*, **8**, 319
- Buchner, S. 2010, *ATel*, **2768**
- Çalışkan, Ş., Ertan, Ü., Alpar, M. A., Trümper, J. E., & Kylafis, N. D. 2013, *MNRAS*, **431**, 1136
- Chung, C. T. Y., Melatos, A., Krishnan, B., & Whelan, J. T. 2011, *MNRAS*, **414**, 2650
- Ciolfi, R., Ferrari, E., & Gualtieri, L. 2010, *MNRAS*, **406**, 2540
- Cordes, J. M., & Lazio, T. J. W. 2002, *arXiv:astro-ph/0207156*
- Cutler, C. 2002, *PhRvD*, **66**, 084025
- Dodson, R., Legge, D., Reynolds, J. E., & McCulloch, P. M. 2003, *ApJ*, **596**, 1137
- Dupuis, R. J., & Woan, G. 2005, *PhRvD*, **72**, 102002
- Espinoza, C. M., Lyne, A. G., Kramer, M., Manchester, R. N., & Kaspi, V. M. 2011, *ApJL*, **741**, L13
- Feldman, G. J., & Cousins, R. D. 1998, *PhRvD*, **57**, 3873
- Ferrari, A., & Ruffini, R. 1969, *ApJL*, **158**, L71
- Harris, W. E. 1996, *AJ*, **112**, 1487
- Harry, G. M., & LIGO Scientific Collaboration. 2010, *CQGra*, **27**, 084006
- Haskell, B., Samuelsson, L., Glampedakis, K., & Andersson, N. 2008, *MNRAS*, **385**, 531
- Haskell, B., Samuelsson, L., Glampedakis, K., & Andersson, N. 2009, *MNRAS*, **394**, 1711
- Helfand, D. J., Taylor, J. H., Backus, P. R., & Cordes, J. M. 1980, *ApJ*, **237**, 206
- Ho, W. C. G., & Andersson, N. 2012, *NatPh*, **8**, 787
- Hobbs, G. B., Edwards, R. T., & Manchester, R. N. 2006, *MNRAS*, **369**, 655
- Jaranowski, P., & Królak, A. 2010, *CQGra*, **27**, 194015
- Johnson-McDaniel, N. K. 2013, *PhRvD*, **88**, 044016
- Johnson-McDaniel, N. K., & Owen, B. J. 2013, *PhRvD*, **88**, 044004
- Jones, D. I. 2010, *MNRAS*, **402**, 2503
- Jones, D. I., & Andersson, N. 2002, *MNRAS*, **331**, 203
- Kaplan, D. L., Chatterjee, S., Gaensler, B. M., & Anderson, J. 2008, *ApJ*, **677**, 1201
- Keith, M. J. 2013, in IAU Symp. 291, Neutron Stars and Pulsars: Challenges and Opportunities after 80 years, ed. J. van Leeuwen (Cambridge: Cambridge Univ. Press), **29**
- Keith, M. J., Jameson, A., van Straten, W., et al. 2010, *MNRAS*, **409**, 619
- Knispel, B., & Allen, B. 2008, *PhRvD*, **78**, 044031
- Knispel, B., Eatough, R. P., Kim, H., et al. 2013, *ApJ*, **774**, 93
- Lazarus, P. 2013, in IAU Symp. 291, Neutron Stars and Pulsars: Challenges and Opportunities after 80 years, ed. J. van Leeuwen (Cambridge: Cambridge Univ. Press), **35**
- Lorimer, D. R. 2008, *LRR*, **11**, 8
- Lynch, R. S., & Bank North Celestial Cap Survey Collaborations. 2013, in IAU Symp. 291, Neutron Stars and Pulsars: Challenges and Opportunities after 80 years, ed. J. van Leeuwen (Cambridge: Cambridge Univ. Press), **41**
- Lyne, A. G., Pritchard, R. S., & Graham-Smith, F. 1993, *MNRAS*, **265**, 1003
- Manchester, R. N., Hobbs, G. B., Teoh, A., & Hobbs, M. 2005, *AJ*, **129**, 1993
- Marshall, F. E., Gotthelf, E. V., Zhang, W., Middleditch, J., & Wang, Q. D. 1998, *ApJL*, **499**, L179
- Mastrano, A., & Melatos, A. 2012, *MNRAS*, **421**, 760
- Melosh, H. J. 1969, *Natur*, **224**, 781
- Middleditch, J., Marshall, F. E., Wang, Q. D., Gotthelf, E. V., & Zhang, W. 2006, *ApJ*, **652**, 1531
- Mours, B., & Rolland, L. 2011, h(t) reconstruction for VSR4, Tech. Rep. VIR-0704A-11, <https://tds.ego-gw.it/ql/?c=8762>
- Ng, C., & HTRU Collaboration. 2013, in IAU Symp. 291, Neutron Stars and Pulsars: Challenges and Opportunities after 80 years, ed. J. van Leeuwen (Cambridge: Cambridge Univ. Press), **53**
- Ng, C.-Y., & Romani, R. W. 2004, *ApJ*, **601**, 479
- Ng, C.-Y., & Romani, R. W. 2008, *ApJ*, **673**, 411
- Ortolani, S., Barbuy, B., Bica, E., Zoccali, M., & Renzini, A. 2007, *A&A*, **470**, 1043
- Ostriker, J. P., & Gunn, J. E. 1969, *ApJ*, **157**, 1395
- Owen, B. J. 2005, *PhRvL*, **95**, 211101
- Owen, B. J. 2006, *CQGra*, **23**, 1
- Palomba, C. 2000, *A&A*, **354**, 163
- Palomba, C. 2005, *MNRAS*, **359**, 1150
- Papitto, A., Ferrigno, C., Bozzo, E., et al. 2013, *Natur*, **501**, 517
- Pietrzyński, G., Graczyk, D., Gieren, W., et al. 2013, *Natur*, **495**, 76
- Pitkin, M. 2011, *MNRAS*, **415**, 1849
- Ray, P. S., Kerr, M., Parent, D., et al. 2011, *ApJS*, **194**, 17
- Röver, C., Messenger, C., & Prix, R. 2011, *arXiv:1103.2987*
- Roy, J., Gupta, Y., & Lewandowski, W. 2012, *MNRAS*, **424**, 2213
- Saz Parkinson, P. M., & Fermi LAT Collaboration. 2013, in IAU Symp. 291, Neutron Stars and Pulsars: Challenges and Opportunities after 80 years, ed. J. van Leeuwen (Cambridge: Cambridge Univ. Press), **81**
- Shklovskii, I. S. 1969, *AZh*, **46**, 715
- Somiya, K. 2012, *CQGra*, **29**, 124007
- Stappers, B. W., Hessels, J. W. T., Alexov, A., et al. 2011, *A&A*, **530**, A80
- Taylor, J. H., & Cordes, J. M. 1993, *ApJ*, **411**, 674
- Tian, W. W., & Leahy, D. A. 2008, *MNRAS*, **391**, L54
- Ushomirsky, G., Cutler, C., & Bildsten, L. 2000, *MNRAS*, **319**, 902
- van Leeuwen, J., & Stappers, B. W. 2010, *A&A*, **509**, A7
- Wang, Q. D., Gotthelf, E. V., Chu, Y.-H., & Dickel, J. R. 2001, *ApJ*, **559**, 275
- Wang, W. 2011, *RAA*, **11**, 824
- Zimmermann, M., & Szedenits, E., Jr. 1979, *PhRvD*, **20**, 351